1972

The effects of chemical etching on the magnetic properties of permalloy films

Hai Young Lee
Iowa State University

INFORMATION TO USERS

This dissertation was produced from a microfilm copy of the original document. While the most advanced technological means to photograph and reproduce this document have been used, the quality is heavily dependent upon the quality of the original submitted.

The following explanation of techniques is provided to help you understand markings or patterns which may appear on this reproduction.

1. The sign or "target" for pages apparently lacking from the document photographed is "Missing Page(s)". If it was possible to obtain the missing page(s) or section, they are spliced into the film along with adjacent pages. This may have necessitated cutting thru an image and duplicating adjacent pages to insure you complete continuity.

2. When an image on the film is obliterated with a large round black mark, it is an indication that the photographer suspected that the copy may have moved during exposure and thus cause a blurred image. You will find a good image of the page in the adjacent frame.

3. When a map, drawing or chart, etc., was part of the material being photographed the photographer followed a definite method in "sectioning" the material. It is customary to begin photoing at the upper left hand corner of a large sheet and to continue photoing from left to right in equal sections with a small overlap. If necessary, sectioning is continued again — beginning below the first row and continuing on until complete.

4. The majority of users indicate that the textual content is of greatest value, however, a somewhat higher quality reproduction could be made from "photographs" if essential to the understanding of the dissertation. Silver prints of "photographs" may be ordered at additional charge by writing the Order Department, giving the catalog number, title, author and specific pages you wish reproduced.

University Microfilms

300 North Zeeb Road
Ann Arbor, Michigan 48106

A Xerox Education Company

The effects of chemical etching on the magnetic properties of permalloy films

by

Hai Young Lee

A Dissertation Submitted to the
Graduate Faculty in Partial Fulfillment of
The Requirements for the Degree of
DOCTOR OF PHILOSOPHY
Major: Electrical Engineering

Approved:

Signature was redacted for privacy.

In Charge of Major Work

Signature was redacted for privacy.

For the Major Department

Signature was redacted for privacy.

For the Graduate College

Iowa State University
Ames, Iowa

1972

TABLE OF CONTENTS

INTRODUCTION

Since Blois (1) suggested the use of uniaxial thin magnetic films for high-speed computer memory elements, extensive research and development has been undertaken in this area.

In order to improve the storage properties of thin magnetic films for memory applications, it is necessary to develop a suitable fabrication technique which results in: maximization of the output signal, the minimization of the drive current requirements, and the maximization of the stability of the device to disturb fields.

The magnetic properties of thin magnetic films can generally be described by three parameters:

1) the anistropy field H_k
2) the coercive force H_c
3) the angular dispersion α_{90}

The quality factor, $Q = H_c/(\alpha_{90} H_k)$, should be maximized, since the higher H_c, the more resistant the memory elements to stray disturb fields, and the smaller $\alpha_{90} H_k$, the smaller the drive current requirements for maximum output.

A higher disturb threshold has, therefore, been of fundamental interest, particularly if it can be achieved while keeping the anisotropy field and the angular dispersion within tolerable margins.

By controlling the fabrication parameters such as material composition, substrate temperature, film thickness, substrate surface, annealing and ternary addition, etc., the magnetic properties of thin magnetic films have been investigated by many researchers.

The 81% Ni-19% Fe Permalloy composition has particularly received the most attention because this composition represents the best compromise between the alloy composition of zero magnetostriction and zero magnetocrystalline anisotropy.

The control of surface roughness of substrate has been a widely-accepted technique to provide the magnetic memory elements with higher disturb threshold. The rougher the surface is, the higher the coercive force is. However, an increase of the angular dispersion also occurs.

Most of methods presently used, have been achieved by coating metallic layers on substrates (2). This determines the surface topography and also the structure of thin films which are deposited. It was observed that large skews were present in films on metallic underlayers, since the effects of an oblique incidence was stronger than on glass substrates (3).

Another method to improve the storage properties of Ni-Fe films was achieved by diffusing a nonmagnetic metal into the grain boundaries of the film (4,5).

Chemical etching has been used to reduce the film thickness uniformly for special purposes such as checking of thickness dependence of coercive force (6), making films thin enough for electron transmission microscope (7), and making grooved films (8), etc. So far the effects of chemical etching on the magnetic properties, H_k, H_c, and α_{90}, has not yet been reported yet.

In this paper the effects of chemical etching on the magnetic properties of magnetic thin films will be presented in detail. Several

different etchants have been used for this study to investigate their different effects on the magnetic properties of as-deposited magnetic thin films.

Experimental and theoretical backgrounds pertaining to the dependence of magnetic properties on deposition conditions, thickness, surface roughness, chemical etching, etc. will be briefly reviewed.

Possible mechanisms by which etching alters the magnetic properties are discussed by examining the electron micrographs and by polishing the etched surfaces with fine alumina powder (0.05 μ dia.). Simple theoretical calculations of coercive force and angular dispersion, based on the surface roughness model, were made to analyze the experimental results.

It will be demonstrated that improvement of the storage properties of magnetic thin films for computer memory elements can be achieved by choosing an optimum chemical etching solution and the results obtained in this study will be compared with other results obtained by different techniques.

BACKGROUND AND REVIEW

General

It is well known that the magnetic behavior of uniaxial anisotropic film can depart significantly from the predictions of the Stoner-Wohlfarth model (9) based on the assumption of a single-domain with complete magnetization coherence at all times.

According to the Stoner-Wohlfarth model, a thin permalloy film with uniaxial anisotropy is expected to reverse its magnetization by uniform rotation, when the critical field for rotation H_k is applied in the easy axis (EA) direction opposite to the magnetization. The experimental EA loop shows that the magnetization reversal take place at a field H_c which can be much less than the rotational threshold H_k predicted by the model. The nucleation and growth of magnetic domains reverses the magnetization (10).

On the other hand, the experimental hard axis (HA) loop for low excitation field is in good agreement with theoretical loop. However, for higher excitation fields the HA loop opens up and it indicates the initiation of some incoherent processes. Also even if a film remains in a single-domain state without domain walls, its behavior still departs from the single-domain, coherent rotation model. The reason for this departure is the presence of magnetization dispersion, or magnetization ripple in the film (11, 12).

Domain phenomena and the phenomenon of magnetization ripple should be taken into account to understand the magnetic behavior of actual films. The origin of magnetization ripple and coercive force can generally be explained in terms of inhomogeneities present in the film.

Uniaxial Anisotropy

The uniaxial anisotropy induced by the application of a magnetic field during film deposition is of greatest fundamental and technological interest in magnetic thin films.

The value of uniaxial anisotropy is strongly dependent on deposition conditions, particularly the substrate temperature, deposition rate, and the composition of the film (13). In Fig. 1, the anisotropy field H_k is plotted as a function of substrate temperature for various compositions. H_k decreases with increasing the substrate temperature and in fact H_k extrapolates to zero at temperatures within about 20°C of the Curie temperature. Fig. 2 shows the anisotropy constant K_u as a function of composition for a substrate temperature of about 250°C. It is clear that K_u passes through a minimum in the vicinity of 85% Ni - 15% Fe composition (13).

The magnetic anisotropy can originate in the shape anisotropy, magnetocrystalline anisotropy, strain-magnetostriction anisotropy, and directional-ordering anisotropy, which can act also simultaneously.

Two mechanisms which can cause uniaxial anisotropy are mainly responsible for these results: directional-ordering and strain-magnetostriction (14). The pair-ordering mechanism is expected to act in films in the same way that it acts in bulk material, except that the annealing time, and temperature may be reduced from the bulk case because of the high atomic mobility prevailing during deposition, and the high defect concentration found in thin films. The uniaxial anisotropy in Ni-Fe due

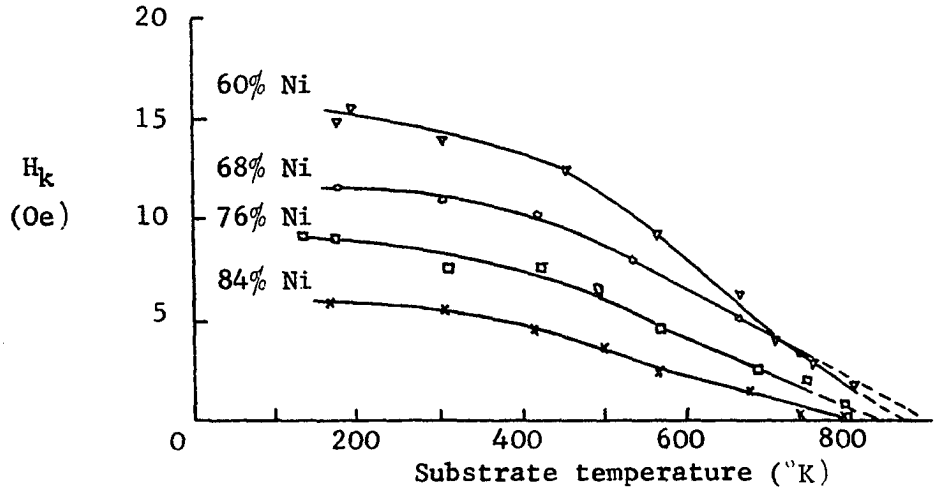

Figure 1. Anisotropy field H_k vs. substrate temperature for Ni-Fe films of various compositions

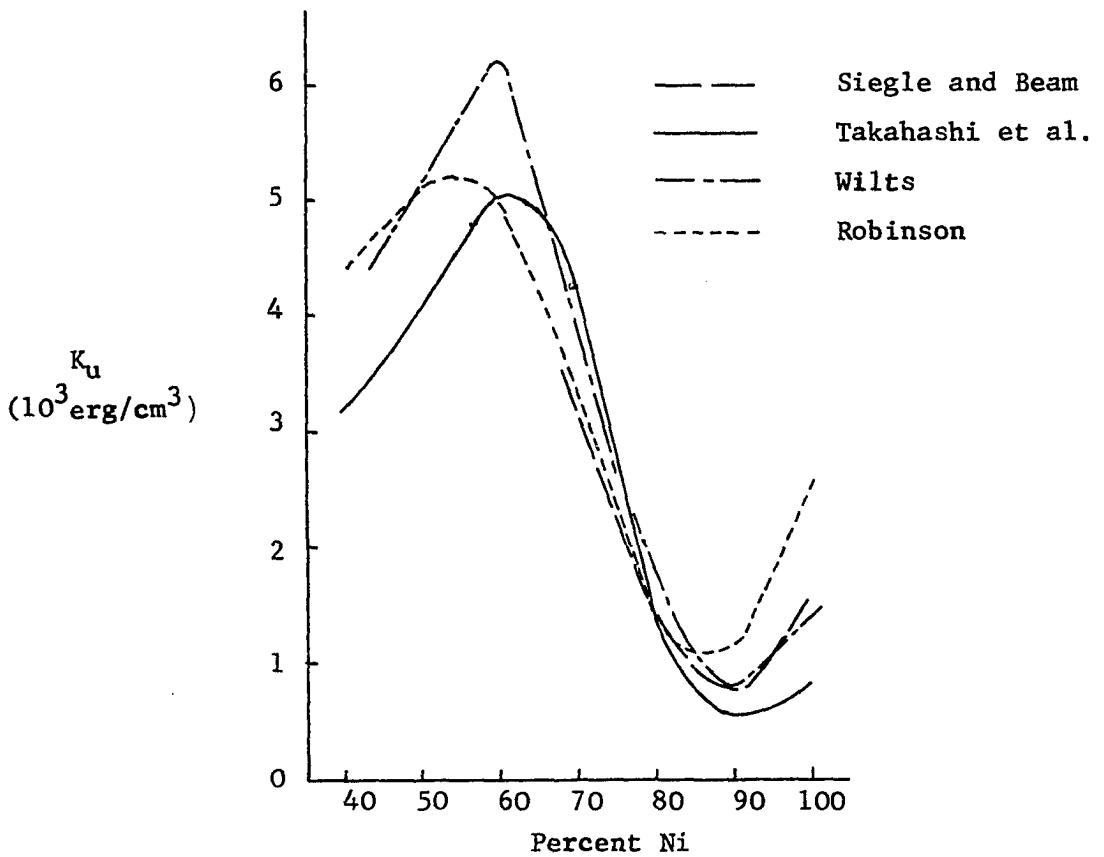

Figure 2. Uniaxial anisotropy constant K_u vs. Ni-Fe composition

to Fe-Fe (or Ni-Ni) pairs is given theoretically by

$$K_u = \frac{AC^2(1-C)^2B^2(Ta)B^2(Tm)}{Ta}$$

The additional contribution to the uniaxial anisotropy comes from the strain-magnetostriction mechanism. At a temperature T, a film which is free from its substrate will sustain a temperature dependent anisotropic strain $\lambda(T)$, the saturation magnetostriction suitably averaged over a polycrystalline film. The direction of this strain is along the magnetization direction and in tensile or compressive according to the sign of $\lambda(T)$ is positive or negative. Assume that as the film is cooled after deposition, a critical temperature T_o is reached below which the atoms lose their mobility, so that the film is constrained by the substrate to maintain the strain $\lambda(T_o)$ at temperatures less than T_o. Thus a stress $\sigma = Y\lambda(T_o)$, where Y is Young's modulus, is exerted by the substrate on the film, and is tensile (compressive) if $\lambda(T_o)$ is positive (negative). At the measuring temperature T_m (usually room temperature) the saturation magnetostriction is $\lambda(T_m)$; since the film is under the stress σ, a uniaxial anisotropy is created with

$$K_u = \frac{3}{2}\lambda(T_m) \cdot \sigma = \frac{3}{2} Y \cdot \lambda(T_o) \cdot \lambda(T_m)$$

The combination of a magnetostrictive contribution and the orientation of iron pairs in the matrix of the nickel lattice gives a semiquantitative fit to the experimental datas because of the difficulties to estimate the values of T_o and T_a, and effects of impurities.

Based on the current theoretical understanding of the induced anisotropy, H_k, should not vary with thickness unless a major contribution arises from an isotropic magnetoelastic or magnetostatic effect which displays a thickness dependence. This can occur if strain relief mechanisms or a change in surface morphology (due to grain boundary grooving, preferred grain growth, etc.) are thickness dependent. These latter effects have not been observed in films less than 1000 Å thick.

Coercive Force

According to single-domain theory, a thin ferromagnetic film with uniaxial anisotropy is expected to reverse its magnetization by uniform rotation, when the threshold field for rotation H_k is applied in the easy direction opposite to the magnetization. In actual films the magnetization reversal is preceded by a wall motion process.

The coercive force H_c for reversal by domain-wall motion, cannot yet be quantitatively predicted. It is clear that inhomogeneities in the film must cause a moving wall to experience a variation of wall energy with position, and thus cause a nonzero value of H_c. Inhomogeneities which can contribute to H_c include spatial variations in film thickness, magnetic anisotropy, magnetization, and the exchange constant. The dependence of coercive force and angular dispersion on film composition is shown in Fig. 3 (15, 16). The minimum value of H_c can be found near the zero magnetostriction composition as angular dispersion does. Thus, it is clear that conditions which lead to low values of magnetization dispersion also favor low values of H_c or vice versa. As can be seen from Fig. 4 of the dependence of magnetic properties on substrate temperatures, coercive force

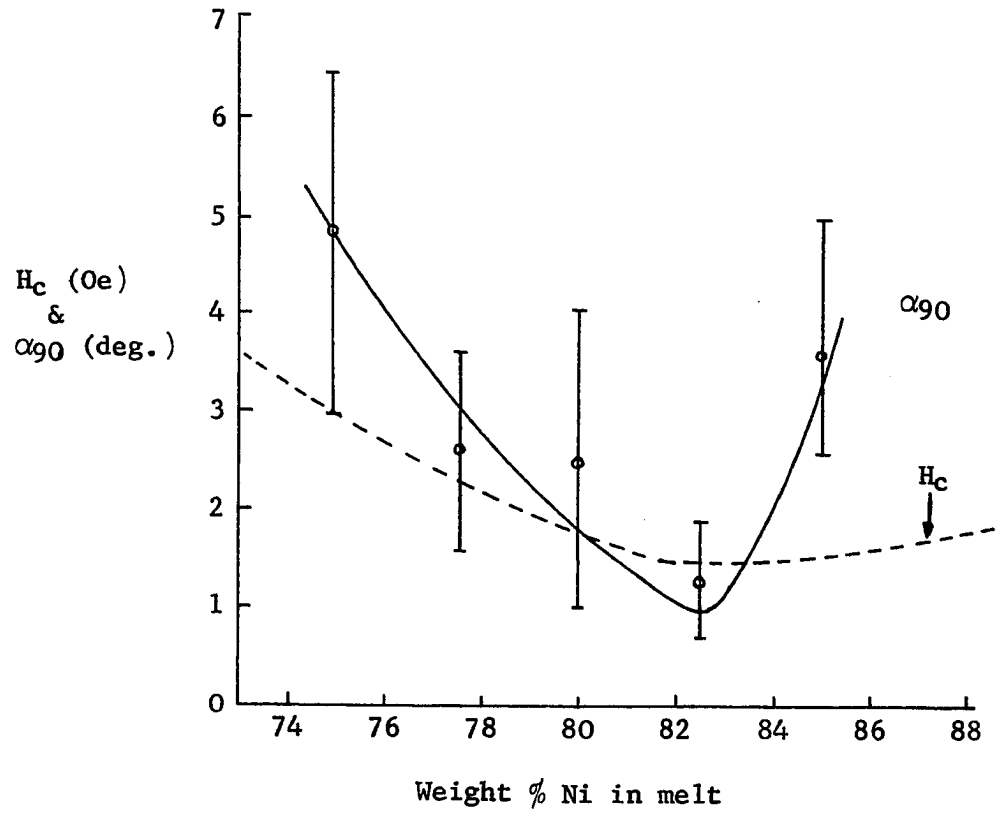

Figure 3. Angular dispersion and coercive force vs. composition

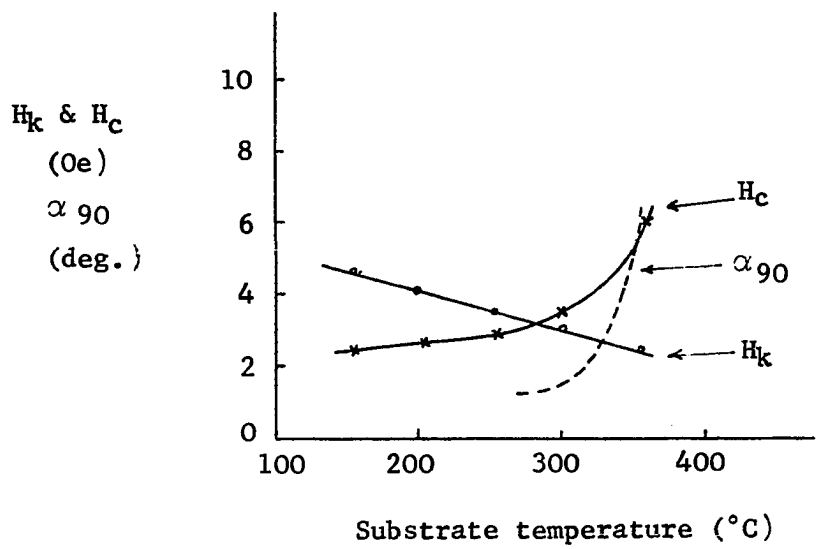

Figure 4. Anisotropy field H_k, coercive force H_c, and angular dispersion α_{90} vs. substrate temperature for permalloy films of zero magnetostriction composition

and angular dispersion increases as the substrate temperature increases (17). A similar experimental result was obtained by magnetic annealing at high temperature (18), too. It is claimed due to the increase of grain size (7) and, the local variation of the anisotropy. Rother (19) reported that a dependence of the magnetization dispersion on the coercive force could be plausible. The effect of inclusions on the domain coercive force of thin ferromagnetic films was investigated by Brice (20). He showed that 2% inclusion by volume could not have a significant increase in H_c, if the diameter of inclusion were smaller than the domain width.

In an early theoretical work (21), the effect of thickness variations due to the surface roughness of a film considered, and it was predicted that $H_c = C\ D^{-4/3}$ in which C is a constant and D is thickness of a film. Several investigators (6,10,22) have measured the thickness dependence of H_c in an effort to check this theoretical prediction. Considerable scatter were found in experimental results, particularly, for the thickness less than around 1000 $\mathring{A}$ and for the thickness greater than 2000 $\mathring{A}$. The former is due to the presence of different types of domain walls (10), the latter is due to the perpendicular anisotropy originated from strain-magnetostriction and the columnar growth of crystallites of the film. It is, also, clear that H_c is sensitive to deposition techniques and its deposition conditions, and that 4/3 law is not generally satisfied.

There is a still a thickness dependence of coercive force for a normal film in the Bloch wall range, $1000\ \mathring{A} < D < 2000\ \mathring{A}$, as

$$H_c = C\ S\ D^{-n}$$

where C is a constant, S is an index for surface roughness, and D is thickness, and n is an exponent which depends on deposition conditions, provided that these deposition conditions are held constant. The exponent n ranges between 0.8 - 1.4 for permalloy films (22-27), 0.8 - 0.3 for Ni - Fe - Co films (28).

The change of wall type with film thickness plays an important role on the thickness dependence of coercive force. There are several types of domain walls (10): Bloch wall, Crosstie wall and Néel wall. For films of thickness greater than around 1000 Å, Bloch walls are found, with alternating sections of opposite polarity separated by Néel lines. At thickness less than 900 Å Néel walls begin to be of comparable energy to Bloch walls, so that various intervals of walls are made of Néel wall segments of alternating polarity. As thickness decreases, the proportion of Néel to Bloch wall length increases, until around 600 Å the wall becomes a crosstie wall. The spacing between Bloch lines increases as thickness continues to decrease, until a pure single-polarity (Bloch-line-free) Néel wall is produced for thickness less than 300 Å.

The peaks in the coercive force vs. thickness can be found at thicknesses which correspond to transitions from Bloch wall to crosstie wall and crosstie to Néel wall, respectively (24).

The importance of the substrate roughness on the magnetic properties of evaporated and electroplated magnetic films has been discussed in many technical articles (2,3,29,30-32). Lemke (29) reported the effects of substrate cleanness on Permalloy films. Prosen et al. (30) were the first to quantitatively relate surface roughness to coercive force and showed that the higher the roughness factor (surface area/geometric area) is, the higher

coercive force results in. Most of earlier papers on surface roughness effects had a lack of discussions about the effect of surface roughness on angular dispersion and coercive force at the same time. Ahn and Freedman (2,3) showed the low-melting-point metals increased surface roughness and, on the other hand, high melting-point metals or SiO have smoothing effects to roughened surfaces. Also, the effects of these underlayers on magnetic properties, H_k, H_c, and α_{90}, were reported.

The control of surface roughness of substrate by coating metallic or nonmetallic underlayers has been a widely accepted technique to provide the magnetic memory elements with higher disturb threshold. However, an increase of angular dispersion also occurs.

Magnetization Dispersion

The single-domain theory must be modified to cover not only domain phenomena but also the phenomenon of magnetization ripple (11,12). Even if the film contains only a single domain, the magnetization is not uniform in direction, but within the film plane it suffers small, quasi-periodic, local angular deviations from its average direction. These local perturbations originate in locally random magnetic inhomogeneities which are usually thought to be associated with the randomly oriented crystallites composing the film. Such local directional deviation is called magnetization ripple and is important in many magnetic phenomena such as Hard Axis domain-splitting (10), Easy Axis locking, rotatable initial susceptibility, and partial rotation (18), etc.

Several workers have measured α_{90} vs. Ni-Fe composition in films. A minimum value of α_{90} is revealed around the composition for zero

magnetostriction 81% Ni-19% Fe (16). But this result does not allow a choice between the magnetostriction and magnetocrystalline anisotropy contribution because the magnetocrystalline constant K_1 is zero at 74% Ni-26% Fe (33). Furthermore, strain-magnetostriction could be important even if the average magnetostriction is vanished, since the local magnetostriction and the local strain, which may be spatially dependent, are important.

Uchiyama et al. (34) found that the long-range (many millimeter) contribution to α_{90} were originated in strain-magnetostriction, while the local contribution originated in both strain-magnetostriction and magnetocrystalline anisotropy. The latter conclusion was based on studies of local α_{90} vs. composition at different substrate temperatures, which showed a minimum α_{90} at the composition for vanishing magnetocrystalline anisotropy only when substrate temperature was high enough to minimize local strains; otherwise the minimum was near the zero magnetostriction composition.

Generally speaking, the higher substrate temperature during deposition increases both H_c and α_{90}, since grain diameter increases with increasing substrate temperature (7). This effect is evidently caused by the increase in the strength of the ripple-inducing perturbations as the sizes of the crystallites in a film are increased and as the uniaxial anisotropy is decreased by higher deposition temperatures. It should be noted that an increase of surface roughness occurs as the size of crystallites increased with increasing the substrate temperatures (35). Wiederman and Hoffman's surface replicas of Ni-Fe films showed not only the increase of grain size, but also the increase of surface roughness of films with

increasing the substrate temperatures (35).

There have been strong indications that the surface roughness may be a significant cause of magnetization dispersion as it does on H_c.

Ahn and Freedman (2,3) have prepared Ni-Fe films on glass substrates which were previously coated with various metallic underlayers. They found gross changes in H_c and α_{90} as the underlayer thickness was varied. Very large values (about 15^o) were observed when the underlayer formed a discontinuous structure of large "island" size. In this condition the underlayer would be expected to produce considerable surface roughness in the magnetic film.

Fisher and Haber (36) have noted a linear relation between α_{90} and the surface density of grains protruding from the film surface. The protruding grains were observed from replicas of the film surface viewed in an electron microscope. Although the authors suggested compositional variations to be the cause, the surface roughness model seems a more likely of the rise of α_{90}.

Iwata et al. (37) reported that the effect of metallic underlayer on the magnetization ripple and that free poles introduced by the surface roughness of the copper underlayer or that of the structure may be a significant cause of magnetization ripple and the ripple generally increased the coercive force of the films (by 1 Oe).

Oredson and Torok (38) have proposed a mechanism in which the surface roughness of the film plays a role, when they analyzed the variations of δH_b with composition in terms of a three-component local anisotropy: magnetocrystalline anisotropy, surface roughness and anisotropic stress coupled with isotropic magnetostriction.

Thickness dependence of angular dispersion in uniaxial ferromagnetic films has not been successfully investigated, since it is very sensitive to deposition conditions.

Clow (39) found out a monotonous increase of angular dispersion with increasing film thickness between 120 Å and 2000 Å. Leaver (40), on the other hand, reported that the angular dispersion is decreased with increasing film thickness from 400 Å to about 3000 Å and then remained constant or slightly increased. The composition of his films were 80% Ni-17% Fe-3% Co. Finally, Crowther (16) found that the angular dispersion was independent of film thickness between 250 Å and 2000 Å. Leaver and Crowther could not explain their results clearly, but explained that Clow's results were attributed to an apparent angular dispersion which is a function of the demagnetizing fields. Daughton and Pohm (41) confirmed theoretically and experimentally the apparent dispersion angle increases with an increasing demagnetizing field and intrinsic angular dispersion. After Hoffman (11) published his magnetization ripple theory, he proposed a different approach to explain the thickness dependence of angular dispersion through the polycrystalline structures by applying his theory.

The micromagnetic theories of magnetization ripple, those developed by Hoffman and Harte, have been worked out in terms of generalized random perturbing anisotropies; the random local anisotropy K.

The possible physical origins (42) which have been proposed by various workers for the random local anisotropy K and the scale of the inhomogeneities are listed as follows:

1) magnetocrystalline anisotropy, where the scale of the inhomogeneity, α, is crystalline size;

2) magnetoelastic effects. These may be divided into two mechanisms: (a) a uniform anisotropic stress, which is normally grown into films and can coupled with the anisotropic magnetostriction in each crystallite resulting in an anisotropy constant; α is again the crystallite size; (b) a random anisotropic stress, which, coupled with the average isotropic magnetostriction, gives an anisotropy with a so far unknown magnitude for α;

3) variation in the direction of the induced anisotropy; this occurs on the scale of the crystallite and may, conceivably, occur larger or smaller scale as well;

4) scratches, holes, and inclusions:

5) chemical inhomogeneities in alloys:

6) surface roughness which contributes through the shape anisotropy of the "hills and valleys" on the film surface. Hence, the random anisotropy K is very much sensitive to the film structure such as grain size, internal stress, surface roughness, crystallographic orientation and texture, impurities etc.

A mechanism in which the surface roughness of the film plays a role is shown in Fig. 5. Each crystallite is supposed to have a roughly convex surface, while in plan the crystallite cross-section may be irregular and, in particular, anisotropic. The microscopic shape anisotropy of that part of the crystallite which projects beyond the film surface could be the source of a local deviation of the magnetization direction. It is assumed in this model that the magnetization direction is held uniform through the film thickness by exchange forces. It is clear that any form of surface roughness can have a similar effect, and the scale of the

anisotropic region could be either larger or smaller than the crystallite size. If the surface roughness is δ, the film thickness D and the lateral dimensions of the projections are a and $a(1+\Delta)$, Oredson and Torok (38) showed that the effective anisotropy constant is

$$K = 0.2 \frac{\pi \delta^2 \Delta}{a\ D} M_s^2$$

Putting $\delta = 100$ Å, $D = 1000$ Å, $a = 200$ Å and $\Delta = 1$ we obtain $K = 2 \times 10^4$ erg/cm^3, a significant figure.

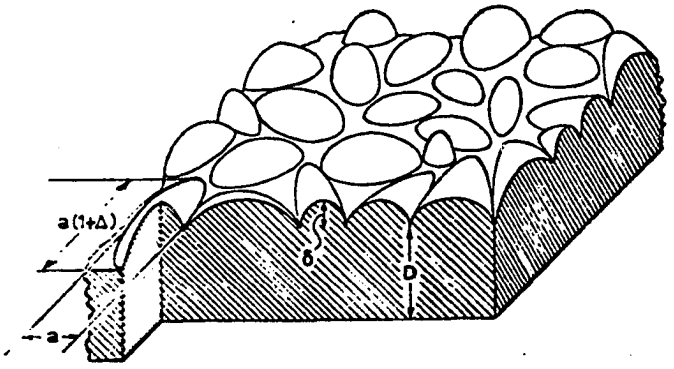

Figure 5. The surface roughness mechanism for local anisotropy

Chemical Etching

Etching is, in general, used for photoengraving arts, printed circuit applications, microelectronics, and metal finishing etc. (13).

Chemical etching has also been widely used for the metallographic laboratory practice (43,44) to reveal the various different features of structures, e.g. grain structures, distribution and identification of

particular phases, orientation of grains, deformation and the effect of strain, and distribution of solute elements of metals and alloys etc.

Etching is fundamentally a selective dissolution process or highly anisotropic dissolution process. Etching solution attacks preferentially high energy areas such as strain centers, chemical inhomogeneities, grain boundaries, or dislocation clusters etc. at significantly different rates.

The reagents used to etch films are principally the same chemicals which are known to dissolve the materials: strong oxidizing agents from the principal group of reagents such as nitric, sulphuric, hydrochloric or chromic acid. For thin film etching, these etchants are applied in fairly dilute solutions to reduce the etch rate.

While aqueous solutions are by far the most common, quite often nonaqueous diluents such as ethyl alcohol, glycerol or ethylene glycol are added to moderate the etching reaction by reducing the dissociation of the active chemicals or by increasing the viscosity of the solution. A group of organic acids such as citric, picric, acetic and oxalic acid is also extensively used in fairly high concentrations because of comparatively weak acidity.

The choice of etching solution is still in an empirical state. Considerable experience has been accumulated with thin film etches for various materials. Only the smaller part of these empirical data has been published, since etch compositions are often carefully kept laboratory secrets. It is good practice to experiment with different etch compositions and adjust them until the best results for the task on hand are obtained. As for etching techniques, immersion with or without agitation

is most common. Etching by immersion method consists of suspending the specimen by means of tongs into a small vessel or petri dish partly filled with the etching solution.

It is necessary that the specimen surface be clean and free from tarnish to ensure even and uniform wetting of the surface by the etching solution. When dealing with freshly deposited and coated thin films, special cleaning techniques prior to etching are rarely required.

Very few technical articles have been reported on chemical etching of magnetic thin films. In 1958 Tiller and Clark (6) etched thin magnetic films in Mirrofe solution in order to reduce film thickness and showed that Néel's prediction of $D^{-4/3}$ dependence of coercive force on thickness agreed with their experiment. They reported that the large surface irregularities were reduced by the etching and the surface roughness was small, by examining electron micrographs of the etched surface.

Anomalous films with rotatable anisotropy were etched in a warm Mirrofe solution and found out the rotatable anisotropy was removed by reducing film thickness (45). By etching anomalous films in ferric chloride acid and analyzing the etched cross section of the film, Prosen et al. (46) proposed a model showing the columnar growth of the alloy normal to the substrate. Recently, Berkowitz et al. (8) investigated a series of grooved uniaxial Permalloy films to determine the influence of controlled thickness variations. Grooved films with etched pattern were obtained by chemical and sputter etching methods. For chemical etching Mirrofe solution was used and the etching rate reported was about 0.5 $\mathring{A}$/sec.

The Mirrofe solution used by the research people mentioned above is an etchant known as nonpreferential chemical etch for iron and steel, commercially available from Macdermid Inc., Waterbury, Connecticut.

Dilute hydrochloric acid was used as an etching solution for evaporated Permalloy films in order to make the films thin enough for a transmission electron micrograph (7). The mean grain size of the films was measured and it was shown the angular dispersion is approximately proportional to grain size.

Tsukahara (47) reported that the ripple were observed most intensely in chemically polished film with the composition between 50 Ni-Fe and 85 Ni-Fe and the ripple was caused by the microscopic shape anisotropy and the stray field anisotropy introduced from the surface roughness.

THEORETICAL CONSIDERATION

Coercive Force

A general theory of the critical field for wall motion in thin magnetic films can formulated in terms of wall energy variation with position. Thus, the coercive force is a function of film inhomogeneities such as surface roughness due to finite crystallite size, local anisotropy variations, contaminations, and imperfections etc.

The wall motion coercive force can be written as

$$H_c = \frac{1}{2 M_s D} \left[\frac{d(\gamma D)}{dx} \right]_{max.}$$

where M_s: saturation magnetization, D: thickness, and γ: surface energy density of the wall.

Assuming the wall energy is a function of exchange energy, anisotropy energy, and stray field energy, it can, furthermore, be written in more extended form as

$$H_c = \frac{1}{2M_s} \left[\frac{\partial \gamma}{\partial K_u} \frac{dK_u}{dx} + \frac{\partial \gamma}{\partial \varphi} \frac{d\varphi}{dx} + \frac{\partial \gamma}{\partial D} \frac{dD}{dx} + \frac{\gamma}{D} \frac{dD}{dx} \right]_{max.}$$

Summarizing, the wall motion coercive force can be generally explained by two roughly independent mechanisms such as magnitude and directional variations of the anisotropy and film thickness variations.

Assuming the contribution of anisotropy dispersion is negligible compared to the contribution of surface roughness, the above expression can be reduced to

$$H_c = \frac{1}{2M_s}\left[\left(\frac{\partial \gamma}{\partial D} + \frac{\gamma}{D}\right)\frac{dD}{dx}\right]_{max}$$

In Figure 6a, the surface energy density of a domain wall as a function of thickness is plotted theoretically (10), assuming $A = 10^{-6}$ ergs/cm, $M = 800$ Gauss, $K_u = 10^3$ ergs/cm^3, while theoretical domain wall widths of Bloch and Néel walls are plotted as a function of film thickness (10). The dashed curve in Figure 6a shows the estimate of crosstie-wall energy density when the Bloch lines is included.

As depicted in Figure 6a, the Bloch wall is energetically more favorable than the crosstie and the Néel wall, for values of film thickness 900 Å. Also, the estimate given in Figure 6a shows that a Bloch-to-crosstie wall transition at 900 Å, and a crosstie-to-Néel wall transition at 200 Å. On the other hand, the wall width of the Bloch wall decreases with decreasing film thickness and does not vary significantly with thickness, as shown in Figure 6b.

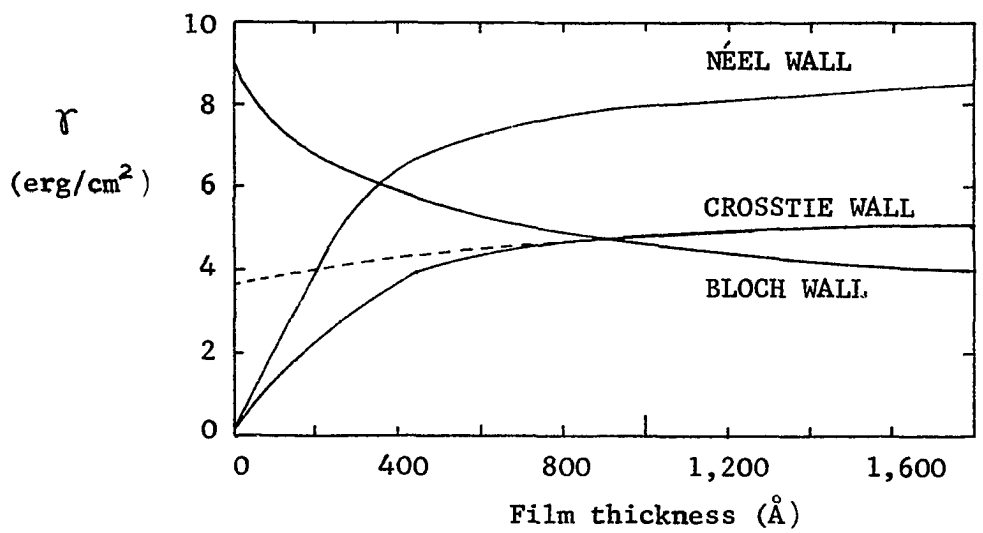

Figure 6a. Theoretical surface energy density γ of a domain wall as a function of film thickness

The width of the Néel wall, in contrast to the Bloch wall, increases with decreasing film thickness. It is noted that the rapid increase in the wall width as film thickness decreases and the wall width ranges from 400 Å to 1.5 μ, as depicted in Figure 6b.

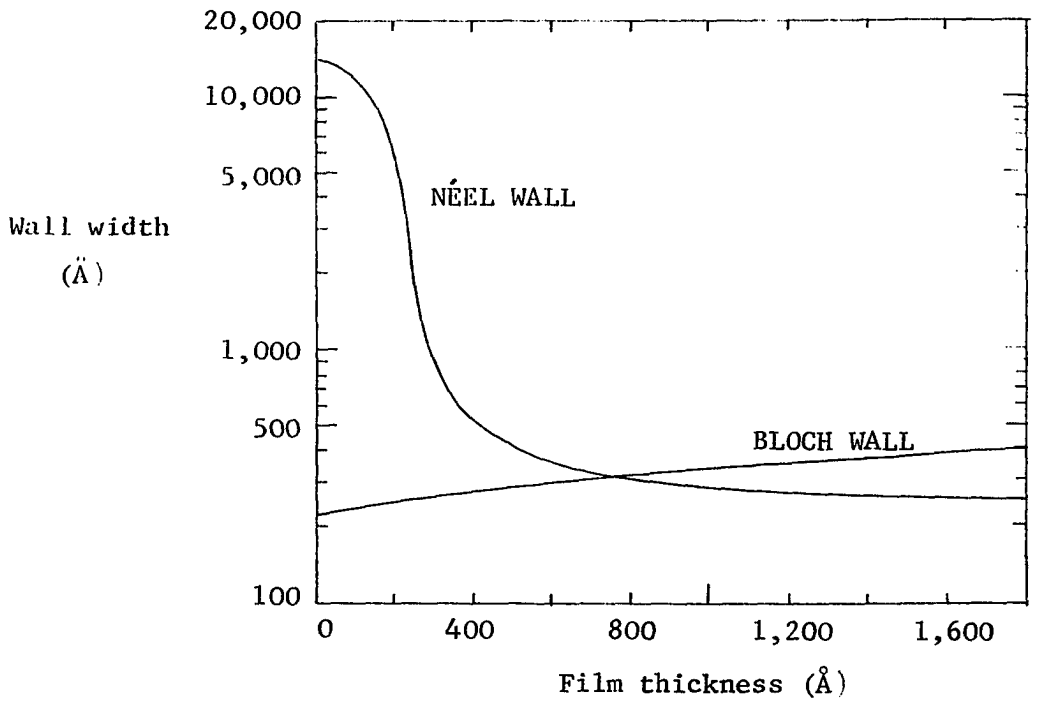

Figure 6b. Theoretical widths of Bloch and Néel walls as a function of film thickness

Consequently, $\left(\frac{\partial r}{\partial D} + \frac{r}{D}\right)$ can be estimated from Figure 6 a, and the theoretical coercive force of a domain wall as a function of film thickness is plotted in Figure 7, assuming the surface roughness to be constant (dD/dx = 0.016), M = 800 Gauss, and the irregularity period of the surface roughness to be comparable to domain wall widths.

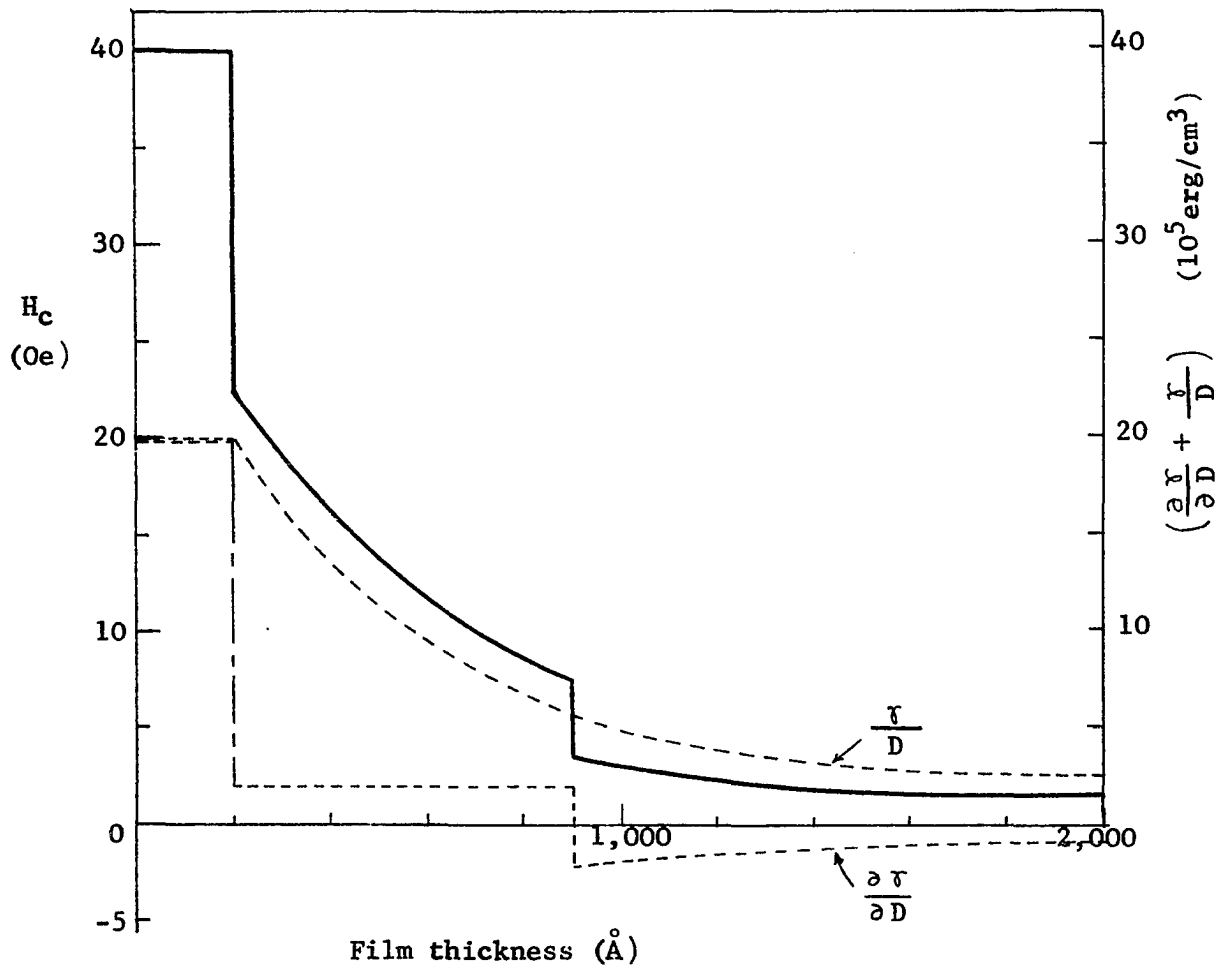

Figure 7. Theoretical coercive force of a domain wall as a function of film thickness, assuming the surface roughness to be constant ($dD/dx = 0.016$), M_S = 800 Gauss, and the irregularity period of the surface roughness to be comparable to domain wall widths

Angular Dispersion

According to the magnetization ripple theory developed by Hoffman, the angular dispersion α_{90} depends upon the structure constant S as

$$\alpha_{90} = \frac{3}{8\pi} \frac{1}{AK_u} S^2$$

where K_u is the uniaxial anisotropy constant, and A is the exchange constant. The structure constant is further related to the random local anisotropy K as

$$S = \frac{KD\sigma_1}{\sqrt{n}}$$

where D is the mean diameter of crystallites, σ_1 a numerical constant of approximately $1/\sqrt{2}$, and n the number of crystallites across the film thickness.

The angular dispersion α_{90} can, therefore, be expressed by

$$\alpha_{90} = \frac{3\sigma_1^2}{8\pi} \frac{D^3}{Ad} \frac{K^2}{K_u},$$

Assuming that the number of crystallites across the film thickness is d/D, where d is the film thickness. Thus the angular dispersion is proportional to the cube of the crystallite diameter and to the square of the random local anisotropy for a film of known thickness and alloy composition.

As previously discussed, the possible origins of the random local anisotropy K can be given by

$$K^2 = K^2_{\text{magnetocrystalline}} + K^2_{\text{magnetoelastic}} + K^2_{\text{surface roughness}}$$

assuming that the magnetoelastic anisotropy is independent of that of the crystalline anisotropy K_1 and K_σ comes from the anisotropic stress σ_a in crystallites.

The magnetocrystalline anisotropy K_1 vanishes at 74-26 Ni-Fe composition and the value at 81-19 Ni-Fe composition is about $-2.0 \times 10^3 erg/cm^3$.

The strain-magnetostriction anisotropy K_σ is given by

$$K_\sigma = \frac{3}{2} \lambda_s \cdot \sigma_a$$

where λ_s is saturation magnetostriction coefficient and σ_a is an anisotropic stress.

The contribution of surface roughness to the random local anisotropy is given by

$$K_s = 0.2 \frac{\pi \delta^2 \Delta}{a\ d} M_s^2$$

Assuming the film has zero magnetostriction composition, the random local anisotropy K can be written as

$$K^2 = K_1^2 + \left(\frac{0.2\pi\delta^2\Delta}{a\ d} M_s^2 \right)^2$$

The angular dispersion is, then, given by

$$\alpha_{90} = \frac{3}{8\pi} \frac{\sigma_1^2 D^3}{AK_u d} K^2$$

$$= \frac{3}{8\pi} \frac{\sigma_1^2}{AK_u} \frac{D^3}{d} \left(\frac{0.2\pi\delta^2\Delta}{a\ d} M_s^2 \right)^2$$

$$= \frac{3\pi}{4} \times 10^{-2} \frac{M_s^4}{AK_u} \cdot \frac{D^3}{d} \left(\frac{\delta}{a} \right)^2 \left(\frac{\delta}{d} \right)^2 \Delta^2$$

assuming the contribution of K_1 is negligible.

The angular dispersion α_{90} is plotted as a function of the surface roughness for zero magnetostriction, as shown in Figure 8, assuming $A = 10^{-6}$ ergs/cm, M = 800 Gauss, $K_u = 10^3$ ergs/cm^3, D = 200 Å, d = 10^3 Å, and $\delta/a = 0.2$.

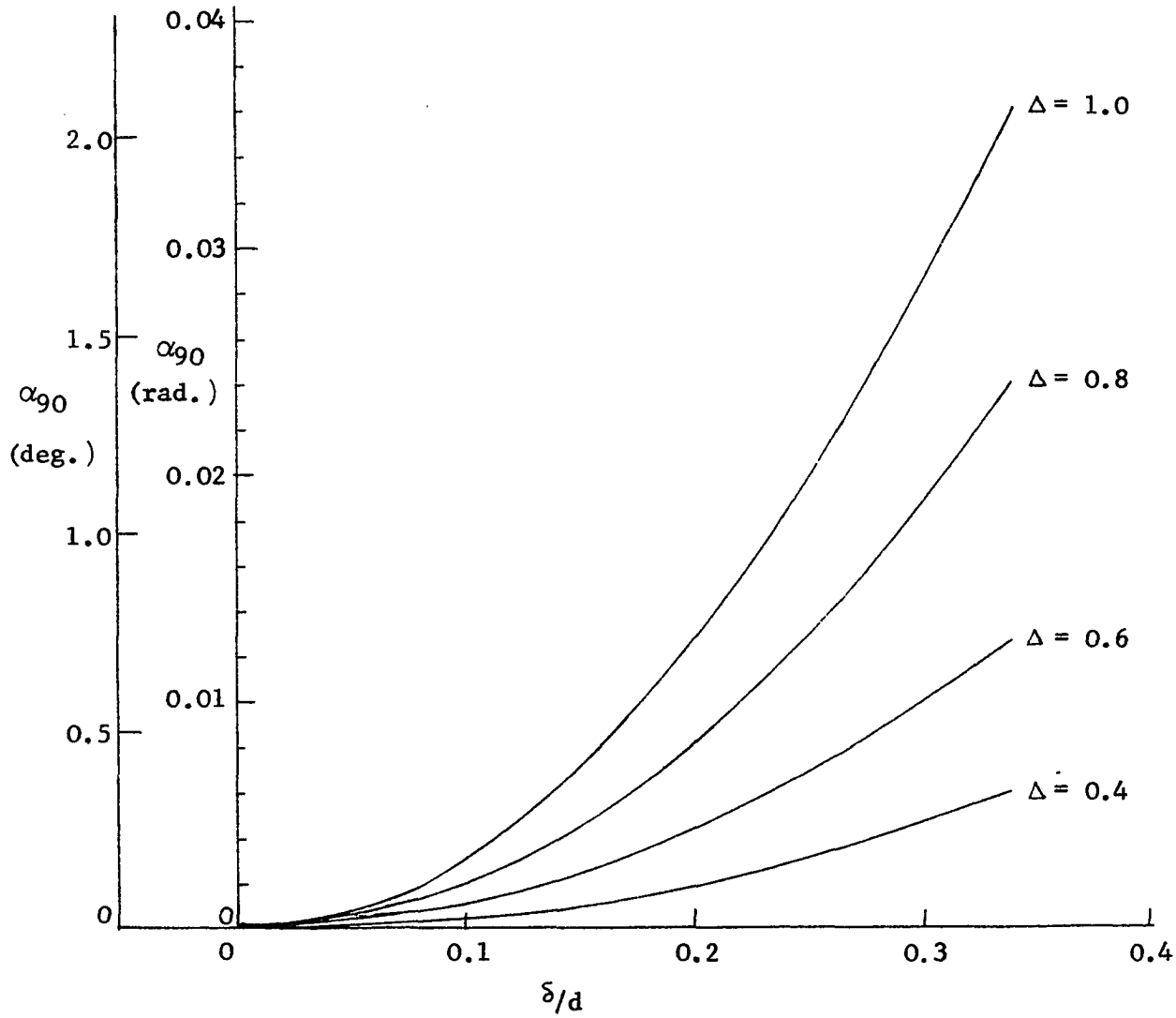

Figure 8. Theoretical dependence of angular dispersion α_{90} on surface roughness

EXPERIMENTAL INVESTIGATION

Fabrication of the Sample Films

The sample films used in this study were made by vapor deposition of Permalloy and Ni-Fe-Co alloy by electron-beam heating. During the deposition and subsequent cooling to room temperatures, a uniform magnetic field of 60 Oe was applied in the plane of the substrate.

Deposition was performed in a vacuum of about 2×10^{-5} torr to assure the mean free path of the vapor molecules in the deposition chamber was longer than the source to substrate distance and to obtain consistent and repeatable results.

The deposition system was a conventional vacuum system (CVC Type LC1-18B) with a large bell jar of 18-inch in diameter and 30-inch in height. A water-cooled, rotatable table was used to hold melt sources and evaporation was performed with a self-accelerated, electrostatically focused electron gun (Veeco, Model VeB-6). A substrate holder was located about 15 inches directly above the melt source to reduce both the thickness gradients in the film and the effects due to oblique incidence of the vapor beam. A mechanically rotatable shutter was also installed just below the substrate holder to avoid contamination during preheating of melt sources.

Temperature of glass substrates was monitored by a pair of iron-constantan thermocouple, placed on a glass substrate and positioned in the substrate holder. Substrate temperature was held at 250°C during the deposition.

A quartz crystal oscillator was used to monitor the evaporation rates and to determine the film thickness. A milli-ampere meter in the high-voltage power supply of the electron-beam gun was also used to control the evaporation rates finer.

Test samples were deposited on Corning cover glass (No. 1, No. 2, 22 mm sq.). Corning cover glass was used as the substrate of specimen because its surface condition is smooth and flat and its thermal expansion coefficient is close to that of Permalloy ($10.6 \times 10^{-6}/^{o}C$ and $12.8 \times 10^{-6}/^{o}C$, respectively). The glass substrates were scrubbed with cotton and cleaned ultrasonically in a warm Alconox solution, rinsed ultrasonically in distilled water followed by a vapor degreasing in hot iso-propyl alcohol vapor and then stored in the degreaser until ready for use.

Permalloy and Ni-Fe-Co were evaporated from an alumina crucible wrapped with a thin tantalum strip. An alumina crucible could hold 3.5 gr of melt. The typical deposition rate was 20 - 30 $\mathring{A}$/sec. at about 200 watts beam power.

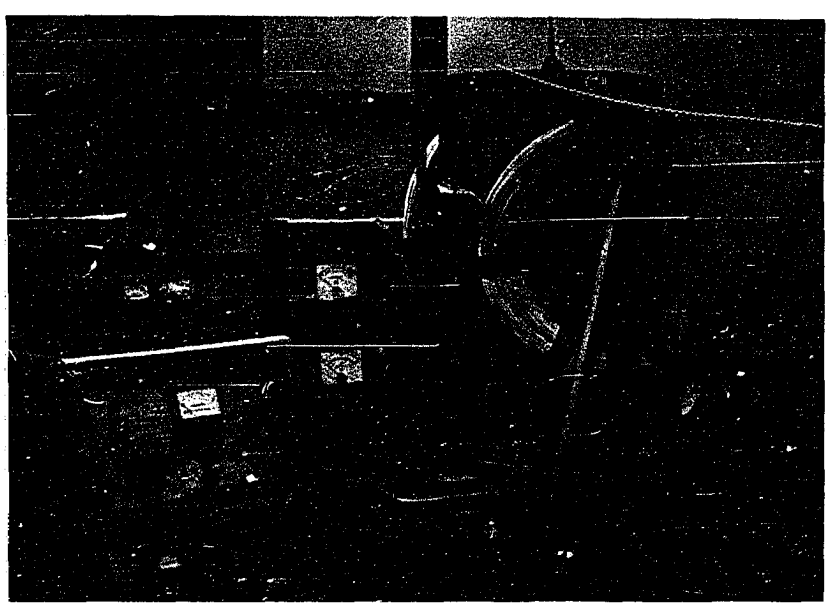

Figure 9. Vacuum deposition systems

Measurements of Magnetic Properties

Because of its experimental simplicity and its ability to measure most of the pertinent magnetic properties, a conventional 60-cycle hysteresis loop tracer is used for examination of magnetic films.

An ac excitation field was produced by a pair of Helmholtz coils whose axis is parallel to the axis of the pickup coil. The separation and the dimensions of the coils were designed to provide a very uniform field in the plane of the film. The film specimen was placed in a rotatable film holder and was then brought into the pickup coil. A bucking coil was also introduced in series with the pickup coil in such a way that the voltage induced by the air flux due to the mutual inductance of Helmholtz and the pickup coil was cancelled by the voltage induced in the bucking coil. In addition, a movable aluminum sheet was also used to balance stray-field disturbances by means of eddy currents induced in it.

The compensated output voltage of the pickup coil, after integration and amplification, was fed to the vertical input of an oscilloscope. On the other hand, a voltage proportional to the excitation field obtained from an 1-ohm resistor in the driving field was fed to the horizontal input of the oscilloscope. Since the height of the hysteresis loop is proportional to both the film magnetization and the film thickness, it could be used to check the film thickness if the scale was precalibrated by a sample film of known saturation magnetization and geometry.

The easy axis loop was used to measure the wall motion coercive force H_c by noting the minimum field for which hysteresis could be detected. The hard axis loop was used to measure the anisotropy field H_k of the

film by extrapolating the initial slope at low transverse field to the saturation magnetization value.

However, this technique of measuring H_k is only valid for low-dispersion films. In films with larger angular dispersion ($\alpha_{90} > 15^o$) the measurement of H_k is often not possible due to open loops in the hard direction.

The angular dispersion or the fallback angle α_{90} was measured by the method suggested by Crowther (48). The measurement of the angular dispersion was made by repositioning the pickup coil so that its axis was perpendicular to the excitation field: the pickup coil then detected the changing flux component normal to the excitation field. A large excitation field greater than H_k was then applied along the hard axis. As the sample was rotated to give a gradually increasing angle α between the hard axis and the excitation field, a signal was measured which increased to a saturation value when M everywhere in the film rotated in the same sense. The fallback angle α_{90} was taken as that value of angle α for which 90% of the saturation signal is measured.

Since there is a discrepancy between melt and film composition in the electron beam evaporation (26, 27) and the magnetostriction is very sensitive to the film composition, magnetostriction measurements were carried out to determine the zero magnetostriction composition of deposited films by the hysteresigraph. A sample film was bent between three sharp knife-edges made from Plexiglass while the value of the anisotropy field H_k was measured as the strain in the sample film was increased by increasing applied stress. Sample films of zero magnetostriction composition would exhibit no changes in the anisotropy field H_k for the applied stresses.

Etching Procedures

A small glass vessel containing an etching solution of known concentration was placed over the pickup coil of the hysteresis loop tracer. Then a sample film to be etched was immersed in the vessel and hysteresis loop on an oscilloscope was observed during the etching period. The changes in coercive force and the height of the hysteresis loop, which indicates the film thickness, were measured. Gradual increase in H_c were observed as film thickness decreased, which could be seen by a reduction of the height of the loop. Also, observing the opening of the hard axis loop, changes in angular dispersion could be roughly estimated.

As will be discussed later, etching rates depend on the concentration, temperature of an etchant, structure and composition of the film, etc. Dissolution depends more sensitive to the temperatures of etching solution than to the concentration of etching solution. Care had, therefore, been taken for the temperature of etching solution to be held constant at the desired value.

The etching activity was also affected very sensitively by aging of etching solution. To get consistent etching results the solution was prepared freshly or aged for a predetermined period of time.

Etched films were thoroughly rinsed in a stream of distilled water for more than five minutes right after taking out of the etch vessel. Absolute ethyl alcohol was used to wash etched films followed by drying in a blast of air.

Prior to making surface replicas for electron microscope examination, etched film surfaces were examined by an optical microscope in order to

look at the microscopic inhomogeneities such as pinholes, uneven etching, or possible stains, since electron microscope examines a quite small spot of a sample film. With oblique illumination, the surface roughness could be indicated by the intensity of randomly reflected lights from film surface. Smooth surfaces looked dark, because of little randomly reflected lights. Rough surfaces were very bright.

Bitter-pattern observations (10) of sample films of as-deposited or etched, were done to look at the magnetization configuration in sample films: domain-wall types gave information about the film thickness, and hard axis domain-splitting and easy axis locking gave valuable informations about the magnetization dispersion in sample films of high angular dispersion and large normalized coercive force h_c. Also the Bitter Solution technique can be used to check the uniformity of thickness, pinholes, scratches, and surface roughness of films. Particularly, the surface roughness could be investigated by examining the distribution of Bitter particles around rough surfaces, since the Bitter particles are sensitive to the regions of high stray fields which originate in areas of high magnetization divergence. Consequently, observations of surface topography by using an optical microscope was enhanced by applying Bitter solution over films.

Table 1 is the list of chemical etching solutions used for this study. The selection of chemical etching solutions was based on following requirements: a) etched surface should be uniform on a macroscopic scale, b) etching solutions should not leave stains or produce lots of pinholes, c) etching solutions should provide microscopic surface roughness by preferential

Table 1. Etching solutions for magnetic thin films[a]

Constituents		Etch Rates (Å/sec.)
Hydrochloric acid Water	1 part 9 - 4 parts	0.1 - 0.2
Nitric acid Water	1 part 49 - 4 parts	20 - 30
Ferric chloride (lump) Water	1 part (sat) 199 - 4 parts	2 - 100
Chemical Polish		
Nitric acid Sulpheric acid Orthophosphoric acid Glacial acetic acid	30 ml 10 ml 10 ml 50 ml	5
Nitric acid Hydrochloric acid Water	1 part 1 part 198 - 2 parts	0.1 - 10
Nitric acid Hydrochloric acid Copper Water	20 ml 20 ml 0.1 gr 160 ml	7
Mirrofe Hydrogen peroxide	1 part 1 part	0.5

[a] The concentration of nitric acid and hydrochloric acid are 70% and 37%, respectively, unless otherwise specified.

etching on grain boundaries of the film, and d) the surface roughness should be produced without a significant removal of film thickness. For

convenience, concentration of etching solution is expressed as the percentage of volume of basic acid to total volume of an etching solution. For example, 10% nitric acid etching solution = (1 part of HNO_3)/9 part of H_2O.

Electron Microscope Study of Film Surface Roughness

Surface roughness attributed to each layer of the film structure was studied with the surface replica technique (49) by means of an electron microscope. Evaporated carbon film replicas were used to improve the resolution. In addition, the carbon also served as a relief agent to prevent the adhesion of the plastic layer to the metal film surface. The possible artifacts caused by the stresses during the stripping process were greatly reduced by this procedure. Shadow casting with germanium was also employed to improve the contrast of the image and to enable to measure the roughness of the surfaces.

On the film surface to be examined, a rather thick layer of three percent Formvar solution was coated, dried and then stripped to eliminate possible surface contamination. Afterward, a thin carbon film of about 50 Å thick was vapor deposited on the specimen as surface replica. Then, a thin layer of one percent Formvar solution was spread on the carbon-coated surface with an eyedropper, and the specimen was held at an angle to allow the solution to drain. When the Formvar film was thoroughly dried, it was scored at the thick end and moisture from the breath was condensed on the film. The moisture seemed to enter the film and facilitated separation of the plastic film with the carbon replica from

the specimen. The plastic-film-backed carbon replica was then cut into small pieces and attached to copper grids, the sample holders for the electron microscope. At this stage, the replica was ready for shadow casting.

Germanium was chosen as shadow casting metal because of its relatively small granularity, ease of evaporation and particularly its high scattering power. It is known that too heavy a coating will obscure fine structures and too small a shadow angle will result in loss of detail behind projections. As a consequence, it is desirable to secure adequate contrast with the minimum thickness of deposit and at a moderate angle of shadowing. Shadow casting with 50 Å germanium at 15 degrees shadow angle, as used throughout this study, showed good results. After shadow casting, the back up Formvar film was then dissolved away completely but slowly by placing the replica-loaded copper grids on a filter paper which was constantly wetted with ethylene dichloride. After this dissolving process, these shadow-casted carbon replicas were then studied by means of an electron microscope.

The micrographs of the replicas indicated that shadow casting with germanium indeed effectively enhanced the visibility of the structure associated with surface elevations and depressions. The relatively sharp shadow resulted from the casting at a large distance provided a simple way of determining the height and the periodicity of the surface irregularity. By measuring the shadow length from the micrographs, the individual height of the surface elevations, could be estimated from the relation

$$h = d \tan \theta$$

in which h is the height of the surface elevation, d is the shadow length, and θ is the shadow angle.

A schematic diagram of surface replica fabrication of a transmission electron microscope study is illustrated in Figure 10.

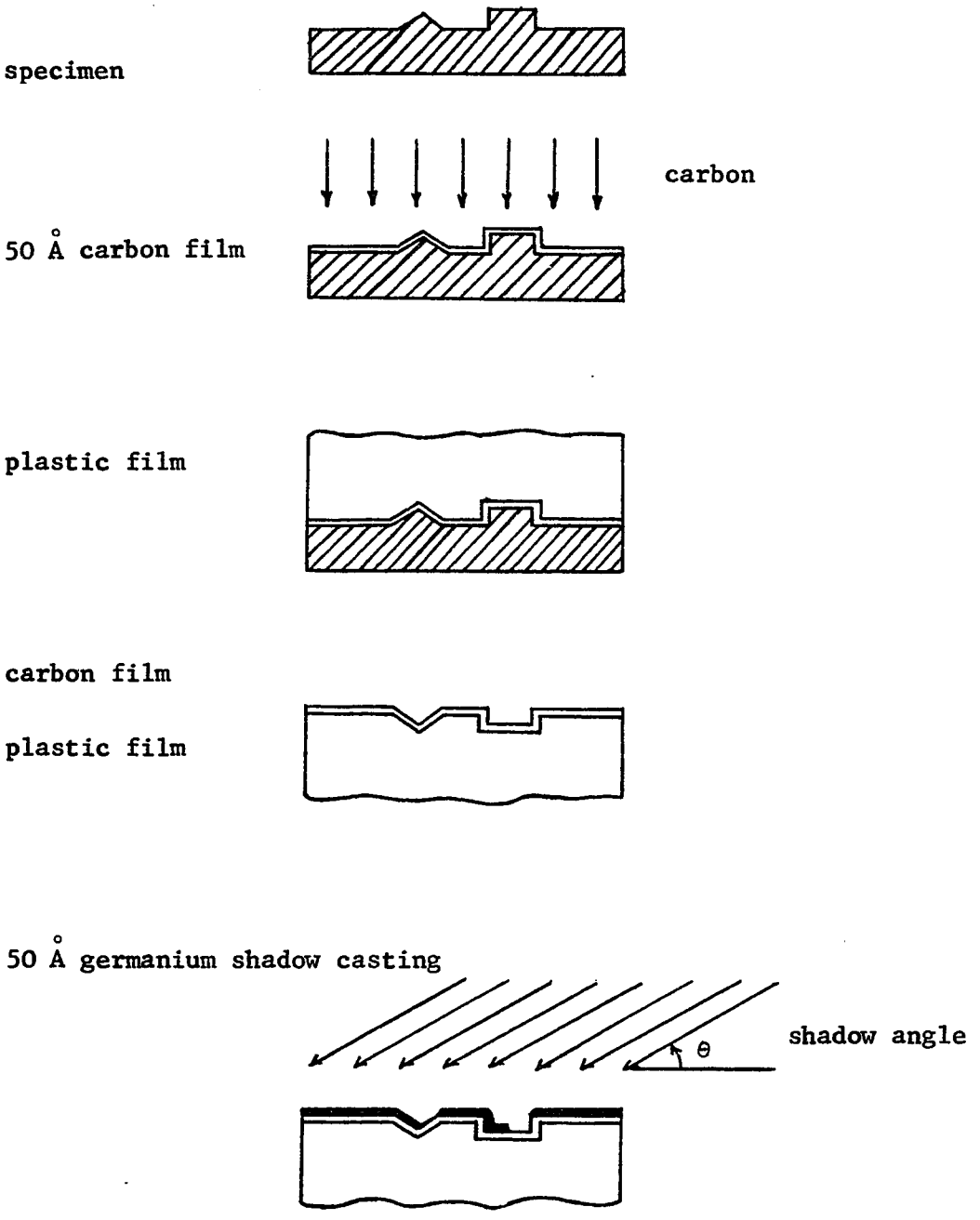

Figure 10. Schematic diagram of surface replica fabrication of a transmission electron microscope study

EXPERIMENTAL RESULTS

The Magnetic Properties of As-Deposited Films

First of all, the magnetic properties of as-deposited films, which were made on the deposition conditons as described in the previous section, are shown in Figures 11, 12, and 13.

Each evaporation had twelve cover-glass substrates (Corning 22 mm sq.). The total range in the parameters and the average value of three or more evaporations (36 or more film samples) were indicated in these figures. This experimental result was needed for the study on chemical etching, because there are no identical deposition systems and data on H_c and α_{90} reported in other papers can not be used to evaluate the thickness dependence of coercive force and angular dispersion of etched films.

The dependence of melt composition on H_k, H_c, and α_{90} was in good agreement with the results reported by Smith (shown in Figure 3). The anisotropy field H_k decreases with increasing nickel content in the melt. Also the coercive force and the angular dispersion shows their relative minimum at 82% - 83% Ni content in melt compositions. The anisotropy field H_k had little variations with film thickness, as shown in Figure 13. The thickness dependence of H_c was, particularly in pattern, agreed well with published data, in the thickness range of 1000 Å to 3000 Å. However, quite a scattering of the data was found in the thickness less than 1000 Å and the result was very similar to that of Pickard et al. (26) which has a minimum at 500 Å. The scatter of angular dispersion was broader than that of coercive force and the thickness dependence of α_{90} was shown in

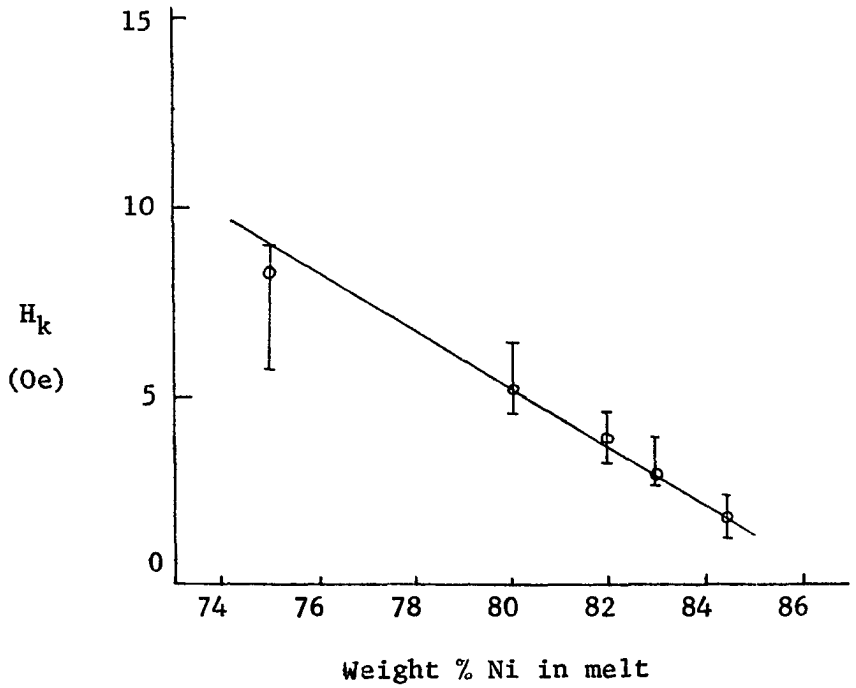

Figure 11. Anisotropy field H_k versus composition

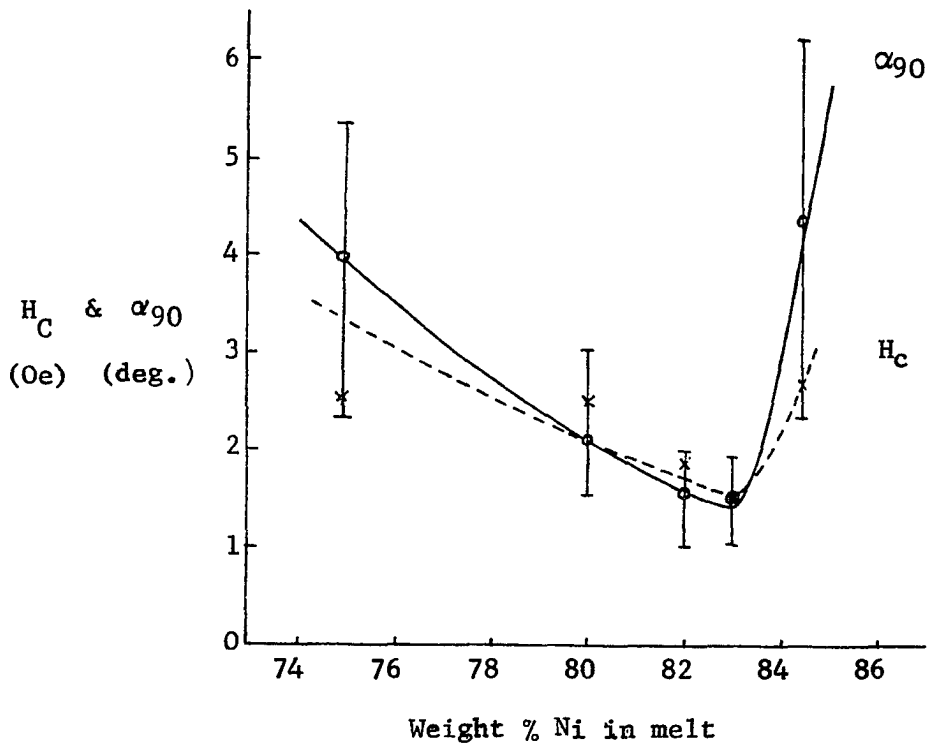

Figure 12. Coercive force H_c and angular dispersion α_{90} vs. Ni-Fe composition

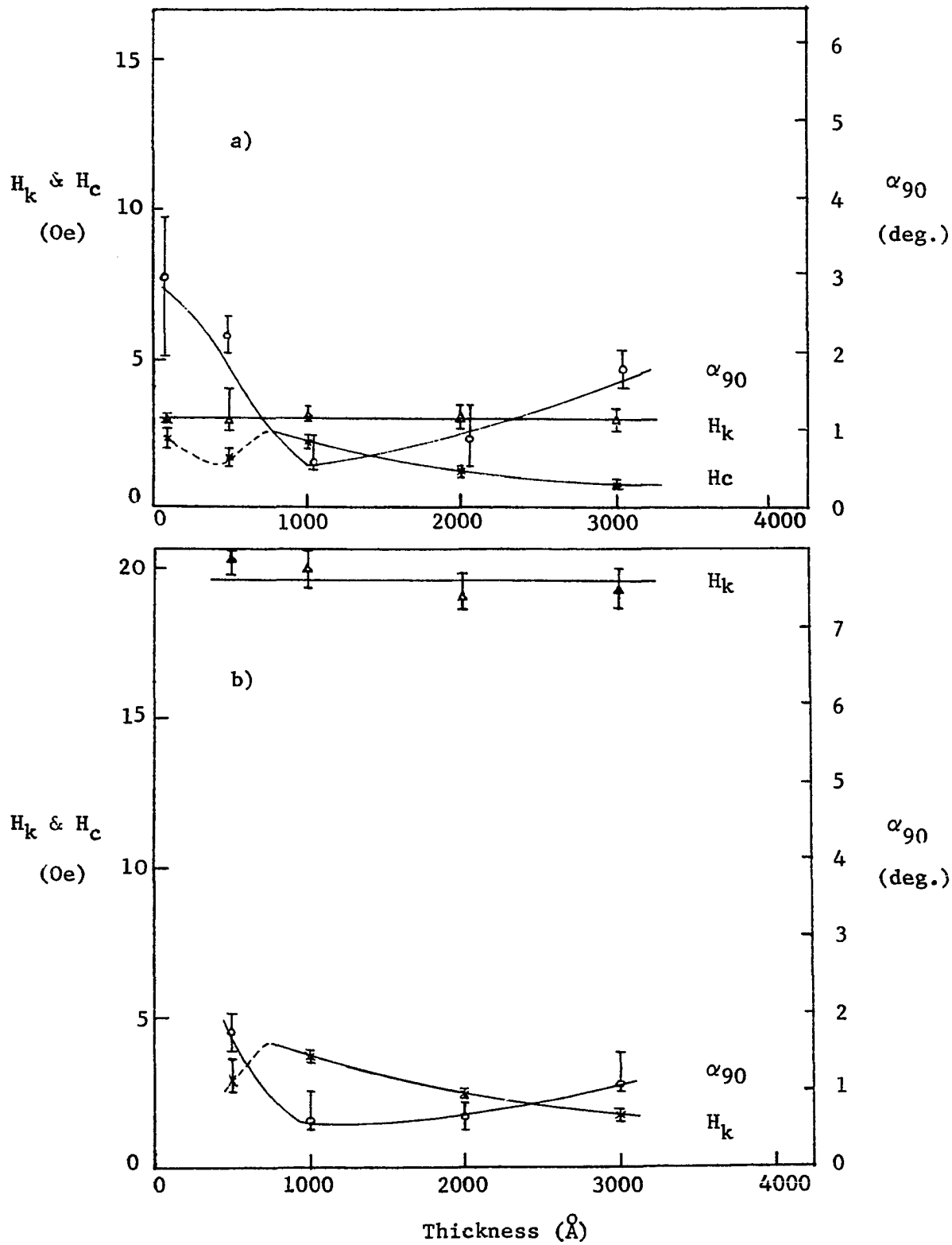

Figure 13. Variation of H_k, H_c, and α_{90} of a) 83-17 Ni-Fe films b) 65-15-20 Ni-Fe-Co films with thickness

Figure 13. However, very thin films with thickness less than 500 Å shows larger angular dispersions.

Effects of $HCl+HNO_3$ Solution

Because of consistency of etching behavior and a fairly good control of etch rates by changing concentrations of the etching solution, more intensive investigation had been performed on the composition of $HCl+HNO_3$ solution. The dissolving power of nitric acid was reduced by adding an equal part of hydrochloric acid.

20% $HCl+HNO_3$ solution found to be an optimum etching solution for 83-17 Ni-Fe and 65-15-20 Ni-Fe-Co films in studying the effects of chemical etching on the magnetic properties. Figure 14 shows the etching rates of different concentrations of $HCl+HNO_3$, HCl, and HNO_3, respectively. In particular, $HCl+HNO_3$ solution had logarithmic increase of etch rates with increasing concentrations of the etchant. As noted in Figure 14, higher etch rates in very low concentrations of 1% and 4% were found unexpectedly. Considerable scatter in the etch rates may be attributed to the structure of films and wetting process of etchant. Etch rates were more sensitive to the temperatures of the solution than to the concentrations of the solution. The dependence of temperatures on the etch rates is shown in Figure 15. Permalloy films having rich iron content had faster etch rates than films containing more nickel, as can be seen in Figure 16. This is attributed to the fact that the activity of nickel is lower than iron. The etch rates were determined by the reduced magnetization flux/etch time, thus the accuracy may be lower than that of microbalance method (50). It can be

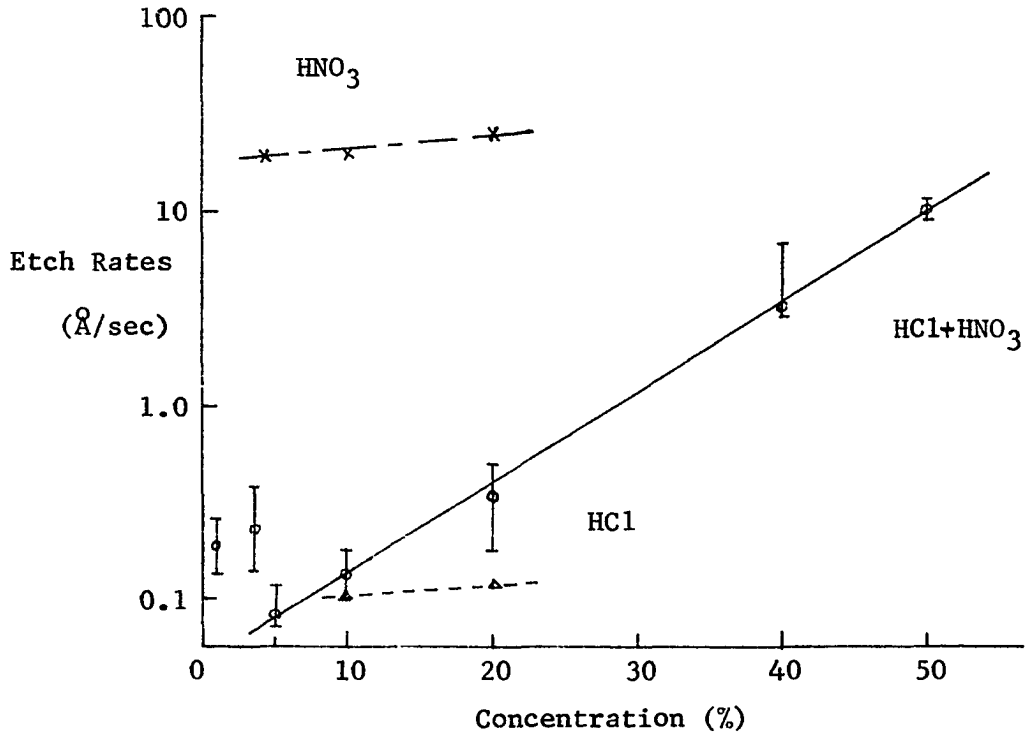

Figure 14. Etch rates of 83-17 Ni-Fe films versus concentrations of $HCl+HNO_3$, HCl, and HNO_3 etching solutions, respectively

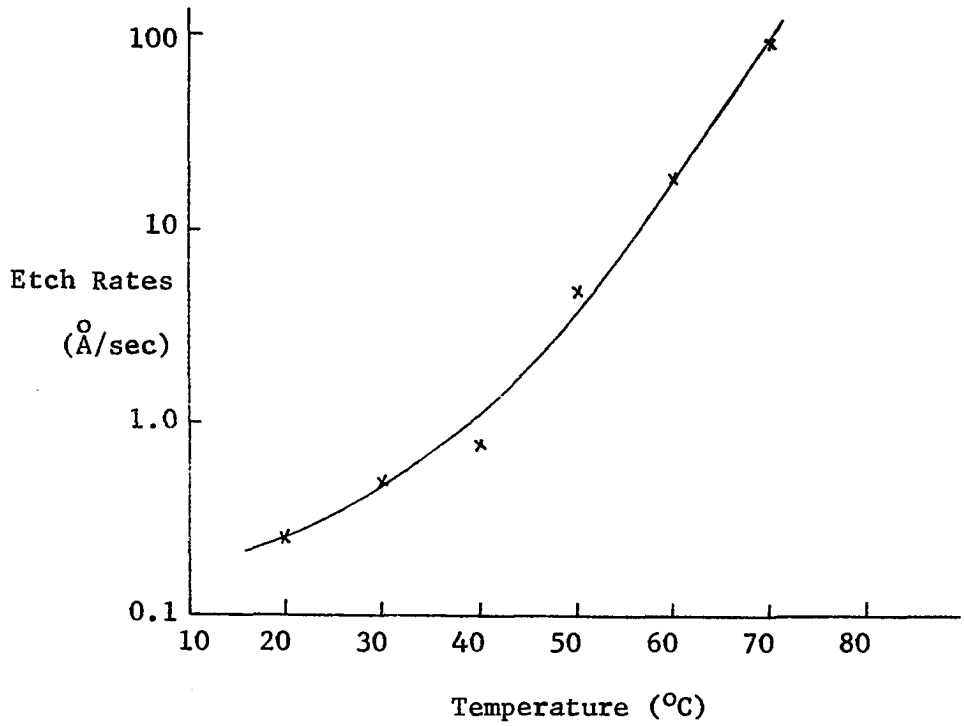

Figure 15. Variation of etch rates with temperatures of etch bath of 20 % $HCl+HNO_3$ etchant

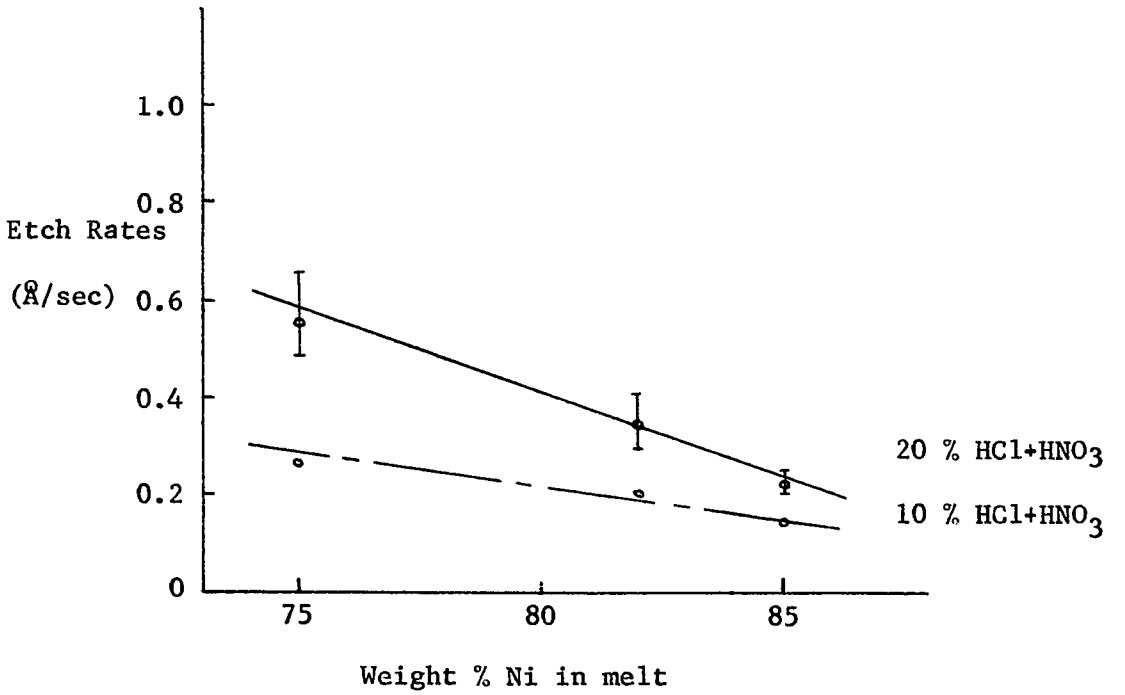

Figure 16. Composition dependence of etch rates on concentrations of etchant

easily seen that films having more nickel content were less sensitive to the variations of concentrations, as shown in Figure 16.

Thin films of various melt compositions were etched in 20% HCl+HNO3 etching solution. The temperature of etching solution was 20°C and the thickness of as-deposited films were around 2000 Å. The etch rates were 0.3 Å/sec. to 0.6 Å/sec., as shown in Figure 16. The etchant was aged for one hour.

Typical variations of the magnetic properties, H_k, H_c and α_{90}, were shown as a function of etch time in Figures 17 and 18. An increase in coercive force was accompanied by an increase in angular dispersion. It was noted that the rate of increase of angular dispersion was relatively small up to a certain point and then it was increased sharply. Figure 25 is a plot of normalized coercive force vs. angular dispersion, where the normalized coercive force is defined as $h_c = H_c/H_k$. Thus it can be easily seen that the sharp increase in α_{90} took place at $h_c \geq 1$. In other words, it occurred when inversions took place; when locking mechanisms took place. The rates of increase in H_c and α_{90} were different for different melt compositions. It was partly due to the fact that films of less nickel content resulted in faster etch rates as depicted in Figure 16, and partly due to other mechanisms of surface inhomogenities.

The behavior of coercive force by the chemical etching is, in many respects, similar to that of Ni-Fe films etched by Mirrofe solution, which was reported by Tiller and Clark (6). It is so, when the coercive force of etched films is plotted as a function of the effective thickness of the etched films. The curve of coercive force vs. effective thickness, as

depicted in Figure 24, could be easily taken for the Neel's 4/3 law (the thickness dependence of coercive force) unless the increase in angular dispersion by the chemical etching had been taken into account carefully. The increase in angular dispersion with etch time cannot be explained either by the apparent angular dispersion which supposed to decrease with decreasing film thickness or Crowther's experimental results which showed no thickness dependence of angular dispersion. Maybe, this discrepancy might be a reason why nobody has ever been tried to study the thickness dependence of angular dispersion by applying the same technique; etching films in Mirrofe solution, as done by Tiller and Clark (6).

Electron micrographs of replicated surfaces of etched films in 20% $HCl+HNO_3$ solution are shown in Figures 21, 22, and 23. Surface roughness was, in general, increased with increasing etch time as can be seen in the surface replicas.

Figure 21 a shows a surface replica of as-deposited films (65-15-20 Ni-Fe-Co, 2000 Å thick). Typical values of surface roughness are ~300 Å in diameter and ~80 Å in height, in average. The typical trend in increasing the surface roughness with etch time is clearly demonstrated in the electron micrographs in Figure 21, as examined on following conditions: as-deposited films of 65-15-20 Ni-Fe-Co, 2000 Å thick, were etched in 20% $HCl+HNO_3$ solution at 20°C for 1000 sec., 2000 sec., and 2500 sec., respectively. As the etch time was increased, the surface roughness became rougher on a larger scale. The resulting changes in magnetic properties and thickness were shown in Figures 17, 18 and 19; thickness was reduced from 2000 Å to 1200 Å, H_c was increased from 2 Oe to 13 Oe, α_{90} from 0.7° to 3.0°, and

H_k remained the same;~15 Oe. A significant increase in coercive force was obtained while angular dispersion had a slight increase. Also, the resulting changes in the surface roughness h/L of etched films for 1000 sec., 2000 sec., and 3000 sec. (etch time) were 100 Å/600 Å, 130 Å/1000 Å, and 150 Å/ 1200 Å, respectively, where h is the average height and L is the average periodicity of rough surfaces.

For Ni-Fe films, the surface replicas of etched films revealed that chemical etching in 20% $HCl+HNO_3$ solution produced not only rough surfaces in microscopic scale, also crater-like pits in microscopic scale, as depicted in Figure 22 c. The size, depth, and density of crater-like pits were increased with longer etch time. Pit sizes ranged from 1000 Å to 20,000 Å (2μ) and the depth was about 350 Å for 1000 sec. etch, 500 Å for 2000 sec. etch. It is noted that the surface roughness inside crater-like pits was smoother than outside whose roughness were 150 Å/600 Å for 1000 sec. etch, 200 Å/800 Å for 2000 sec. etch. The occurrence of crater-like pits is most likely caused by the existence of possible strain centers throughout the film, since chemical etching is known to be sensitive to grain boundaries, strain centers, chemical inhomogeneities, pinholes, grain boundary oxidation, inclusions, and voids, etc.

Although crater-like pits were produced, the effects of chemical etching on the magnetic properties were practically not different from those of 65-15-20 Ni-Fe-Co films, as depicted in Figures 22 and 23. A significant increase in coercive force was obtained while angular dispersion was increased moderately until inversion took place. The anisotropy field H_k remained at the value of as-deposited films unless the measurement of H_k was not possible due to the opening in the hard direction.

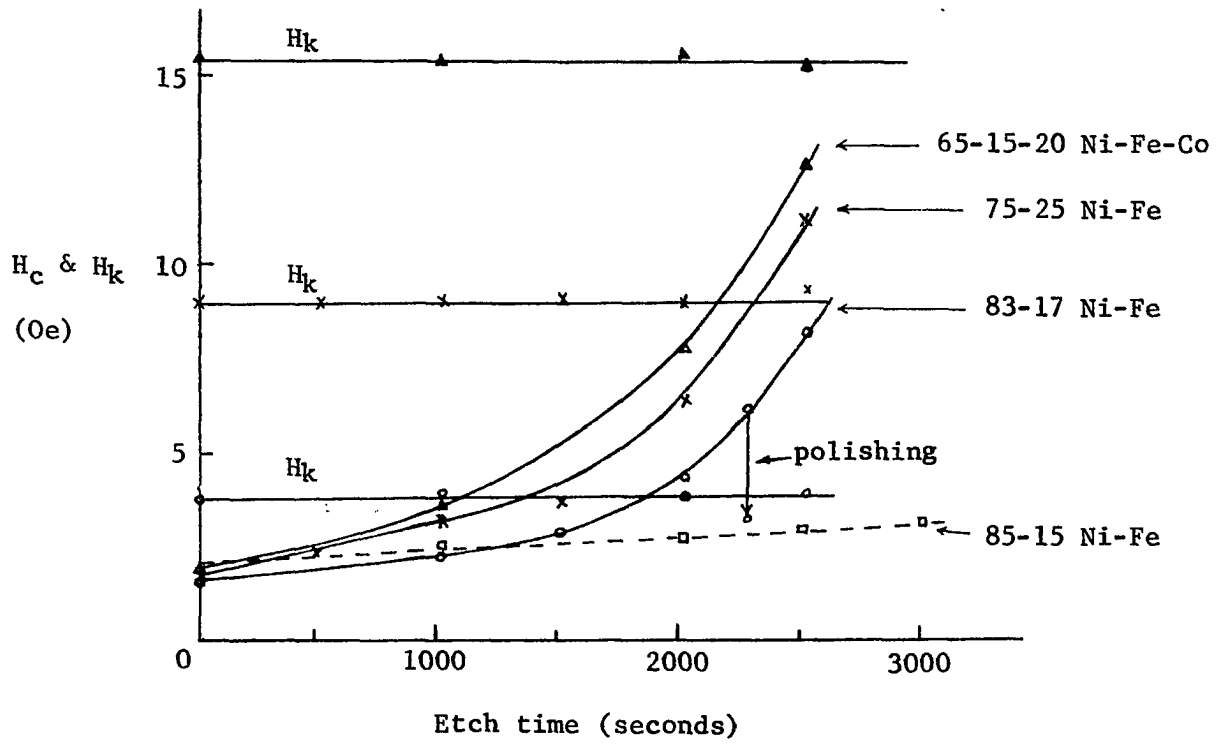

Figure 17. Change in coercive force as a function of etch time

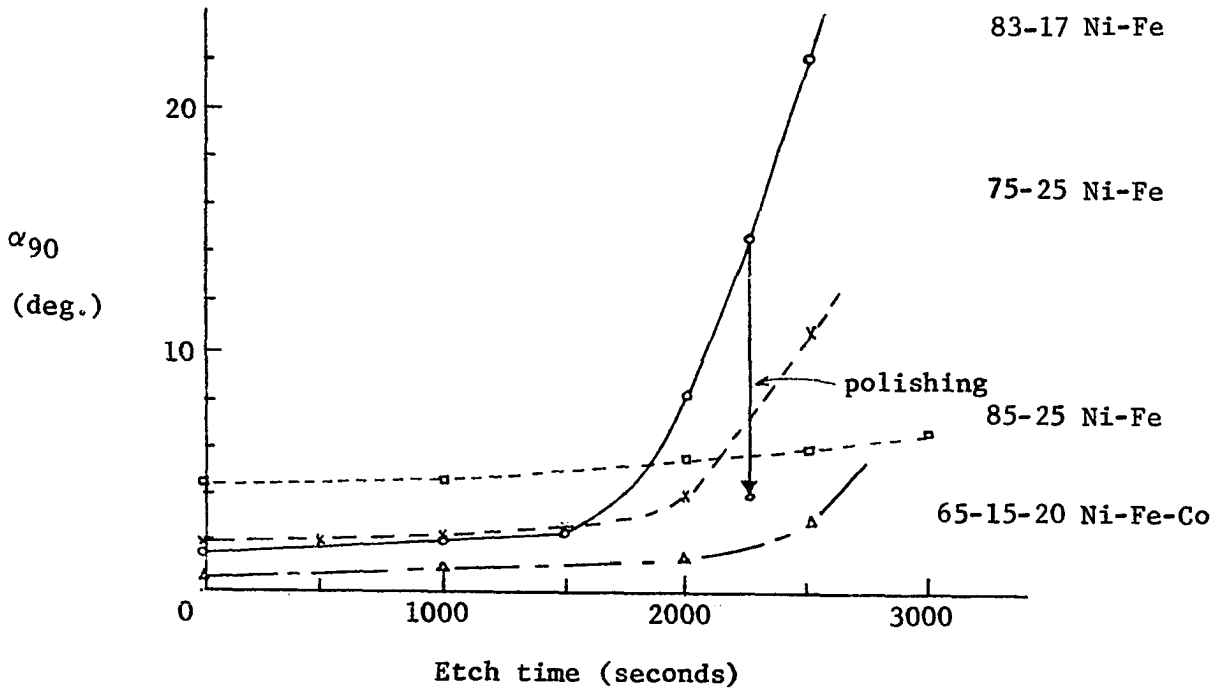

Figure 18. Change in angular dispersion as a function of etch time

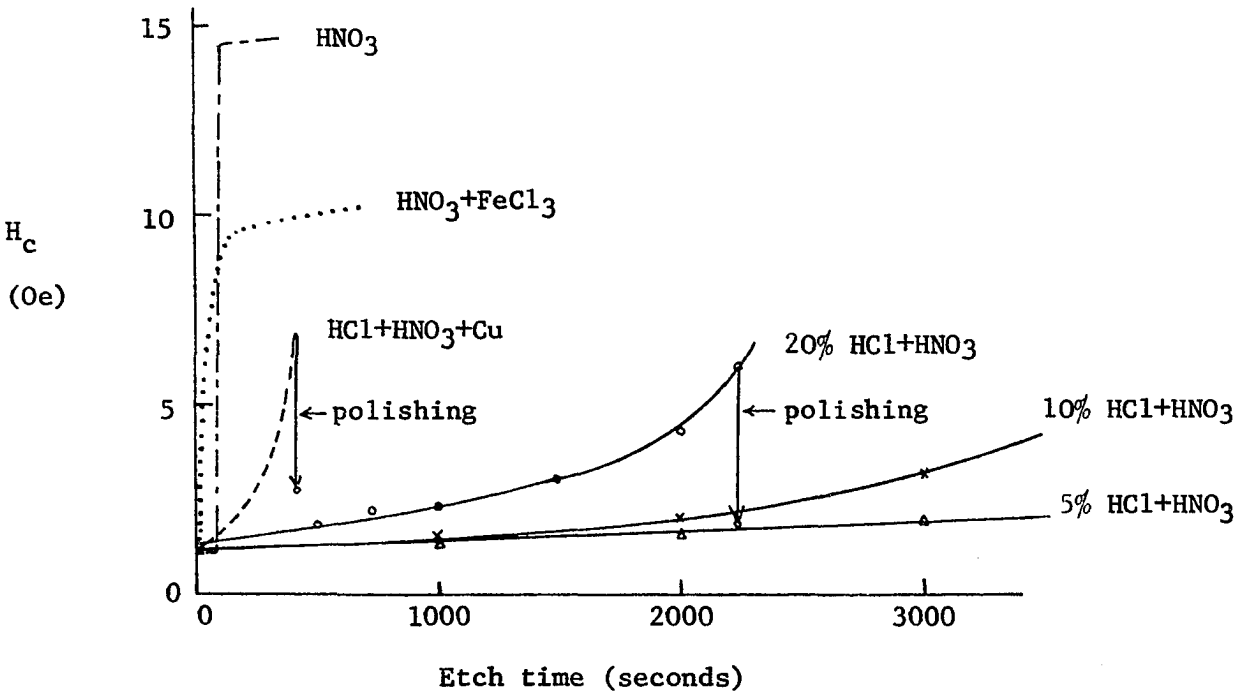

Figure 19. Variation of coercive force for different etching solutions

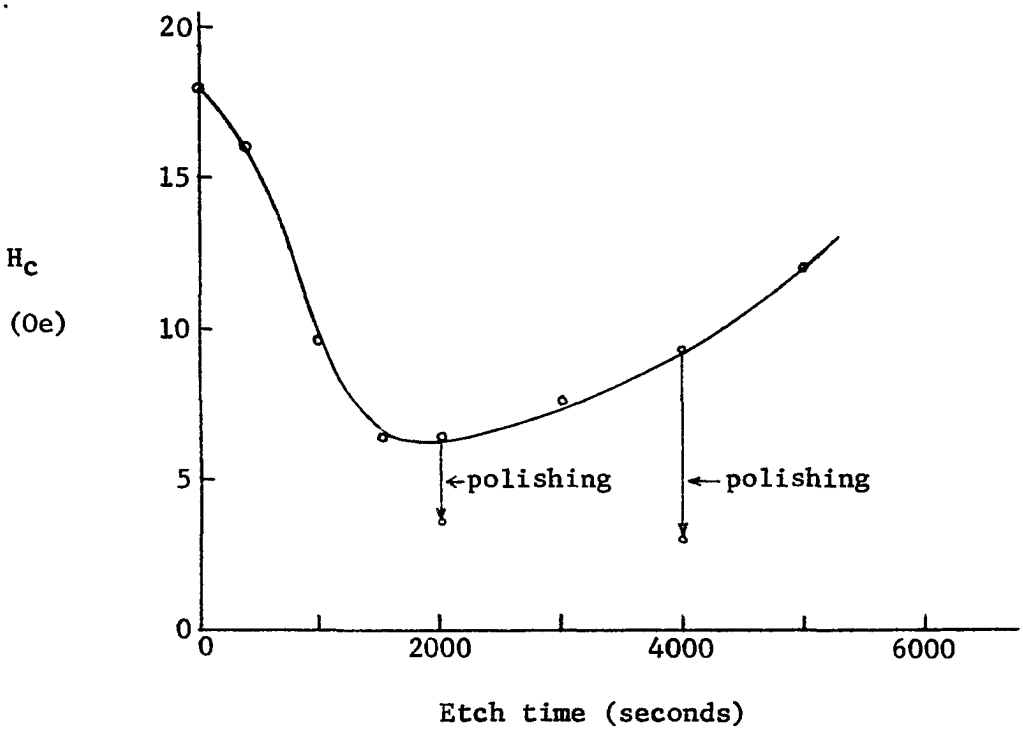

Figure 20. Change in coercive force of an anomalous film as a function of etch time

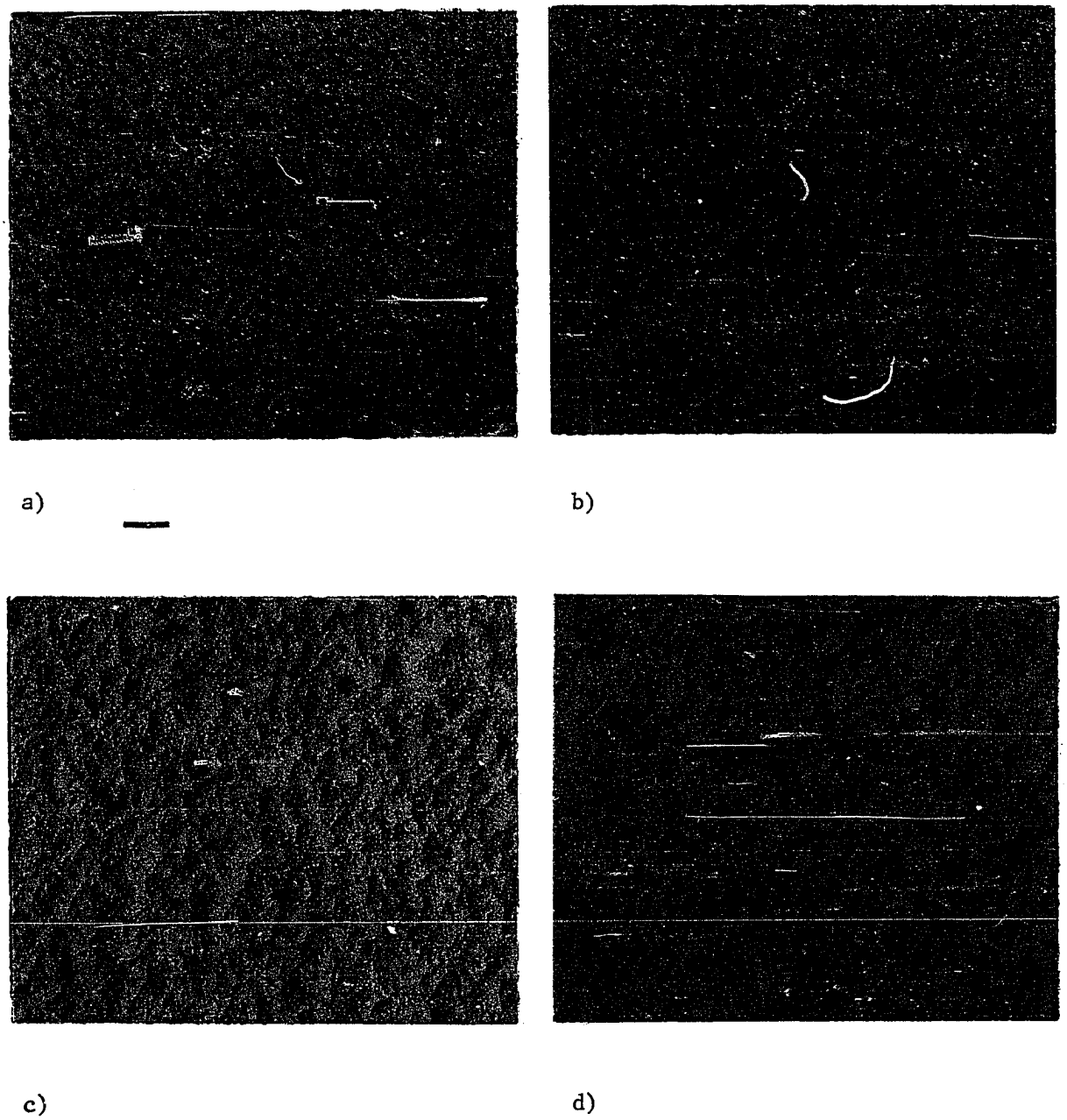

a) b)

c) d)

Figure 21. Electron micrographs of replicated film surface structures of
a) as-deposited film (65-15-20 Ni-Fe-Co 2000 A, x 70,000)
b) etched film (1000 sec. in 20% $HCl+HNO_3$, x 70,000)
c) etched film (2000 sec. in 20% $HCl+HNO_3$, x 70,000)
d) etched film (2500 sec. in 20% $HCl+HNO_3$, x 70,000)

a)

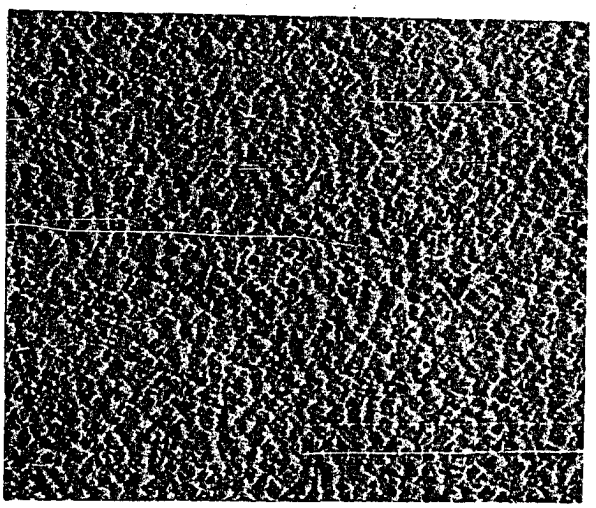

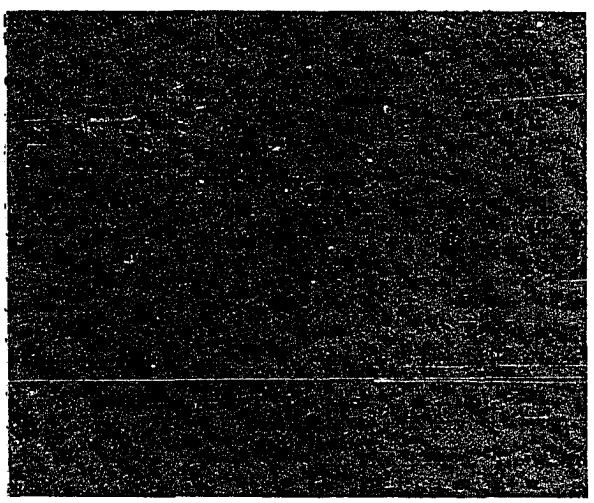

b)

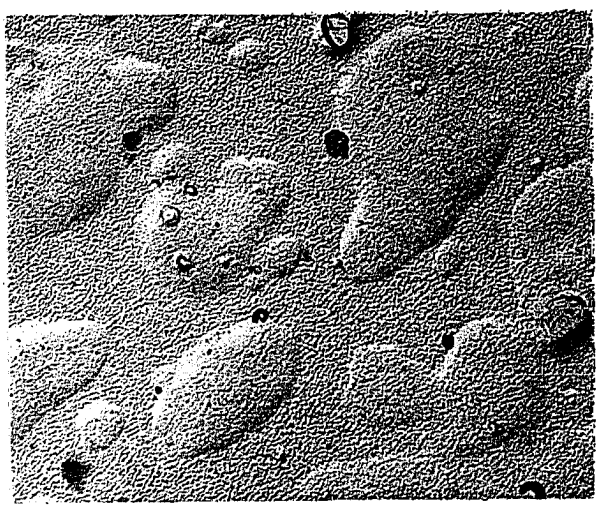

c)

Figure 22. Electron micrographs of replicated film surfaces of
a) 83-17 Ni-Fe, 2000 Å, as-deposited film (x 70,000)
b) 83-17 Ni-Fe, 2000 Å, etched film (1000 sec. in 20% $HCl+HNO_3$, x 70,000)
c) the same as b) but different magnification (x 17,500)

a)

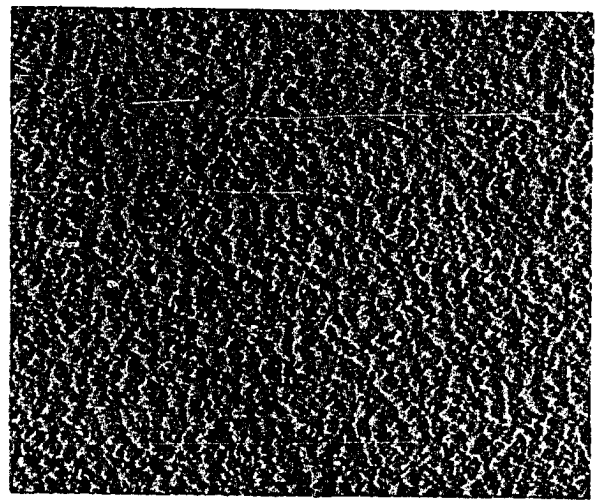

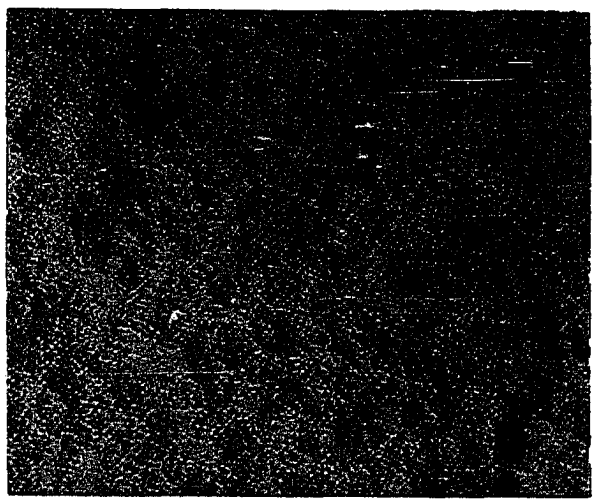

b)

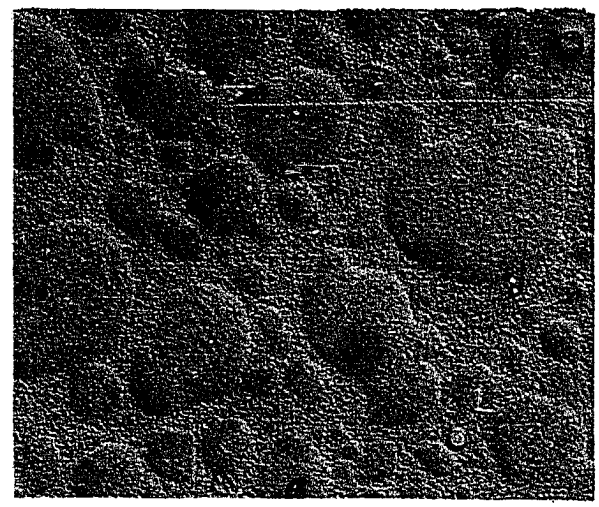

c)

Figure 23. Electron micrographs of replicated film surfaces of
a) 83-17 Ni-Fe, 2000 Å, as-deposited film (x 70,000)
b) etched film of a), 2000 sec. in 20% $HCl+HNO_3$, x 70,000
c) the same as b) but different magnification (x 17,500)

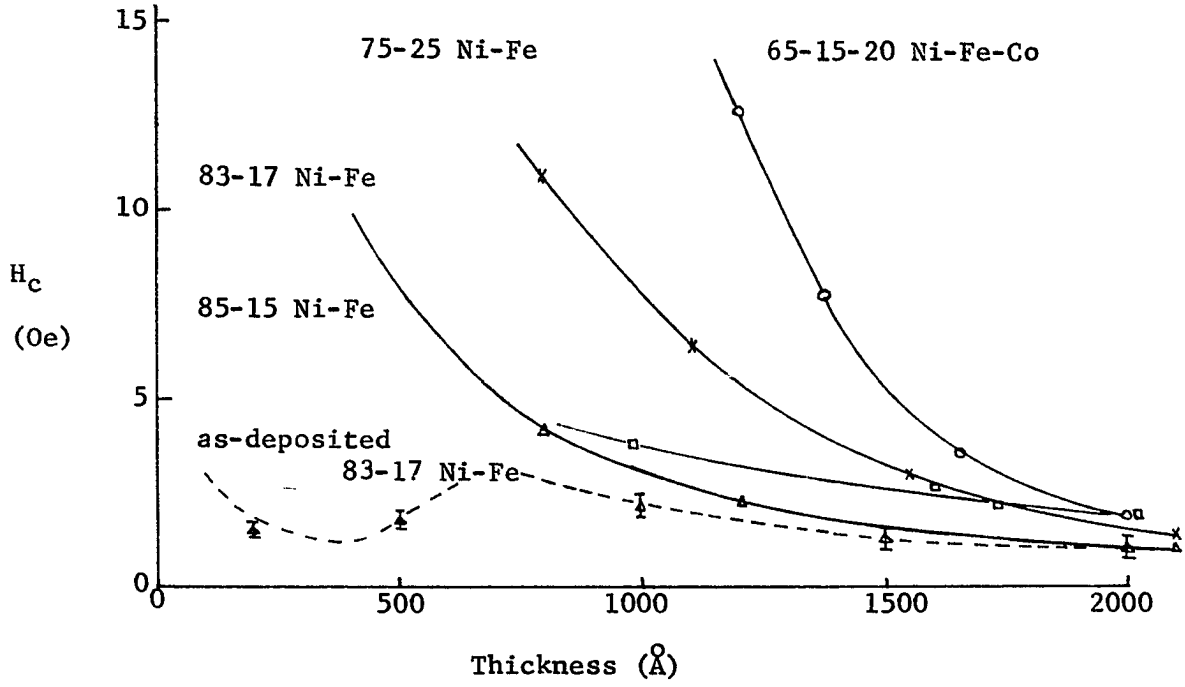

Figure 24. Variation of coercive force of etched films with thickness

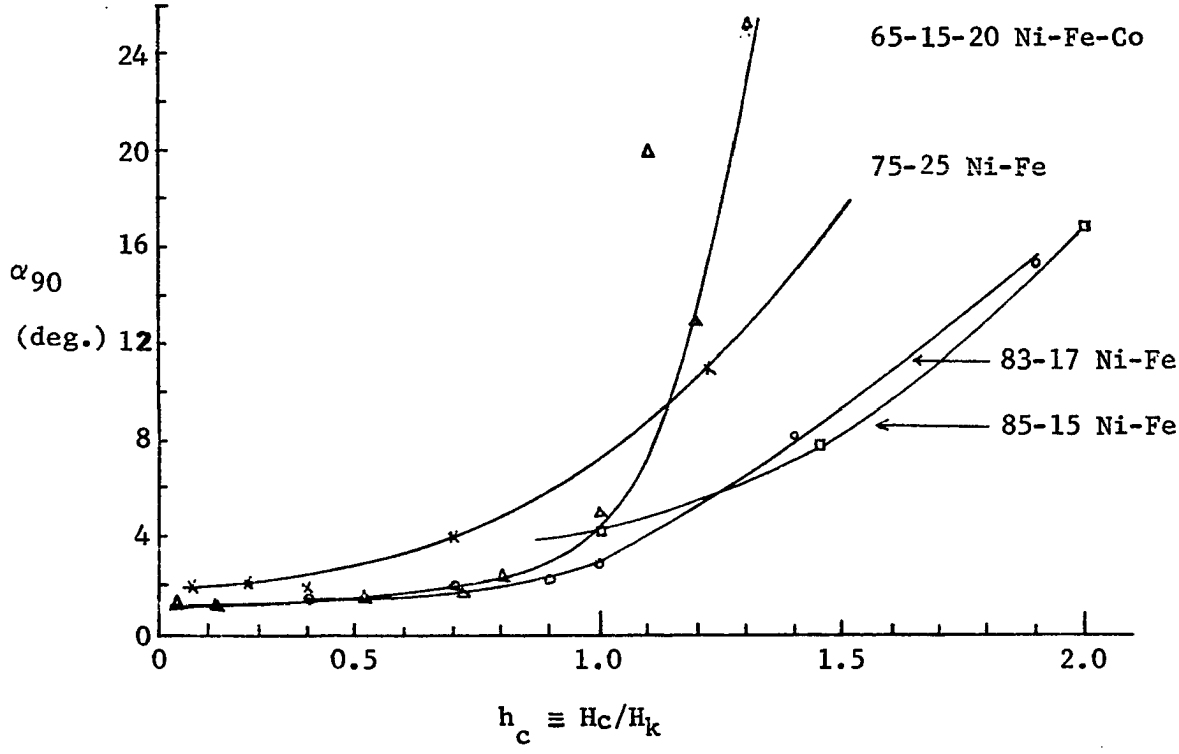

Figure 25. Normalized coercive force h_c versus angular dispersion α_{90}

Anomalous films (25) were obtained at the thickness >~3000 Å for 83-17 Ni-Fe films and >~4000 Å for 65-15-20 Ni-Fe-Co films, when thicker films were evaporated for the study of the thickness dependence of coercive force. These films were also etched and the results were valuable to evaluate the etching mechanisms of chemical etching. Anomalous films can be normalized by reducing the film thickness thinner than the critical thickness. The coercive force decreases monotonically until the film thickness is about 1800 Å, and then the coercive force increases as etching continues, as observed in Figure 20. It was found that the minimum values of coercive force were determined by which kind of etching solution was used. This result is similar to that of Prosen et al. (50). They etched anomalous films in dilute Mirrofe solution. The surface replicas of normalized films (typical easy-axis and hard-axis hysteresis loop can be observed) are shown in Figure 32. It shows that a considerable amount of surface roughness was produced during the removal of film thickness less than the critical thickness. The subsequent polishing of the normalized film could further reduce the coercive force and the angular dispersion of the film, as indicated by arrow in Figure 20. The electron micrograph of the polished film surface is shown in Figure 32 d. It manifests that most of surface roughness produced by chemical etching was removed by polishing. The changes in coercive force and angular dispersion were from 6.4 Oe to 4.7 Oe and from 19° to 3°, respectively.

Effects of Hydrochloric Acid

Dilute hydrochloric acid has a weak dissolving power. Etch rates was about 0.1 Å/s for 10% and 0.2 Å/s for 20% concentration. Surface replica

of films etched in dilute hydrochloric acid shows that hydrochloric acid smoothes the film surface in a certain extent, but produces a comparably large pits. Figure 26 b shows the etched surface of 83-17 Ni-Fe film for 6000 seconds in 20% HCl solution. Its etch rate was 0.13 Å/s and the coercive force was increased from 0.7 Oe to 1.4 Oe and the increase of α_{90} was 0.5° (from 1.5° to 2.0°).

Effects of Nitric Acid

As previously mentioned, dilute nitric acid dissolves readily iron, cobalt and nickel in the written order. Its etch rates ranged in 20 Å/s for 2%, 30 Å/s for 20% concentration, Dilute nitric acid produced very rough surface of grain size in 1000 Å diameter as can be seen in Figure 27. Figure 27 b and c reveals the surface topography of etched films of 83-17 Ni-Fe in dilute nitric acid of 10% and 4%, respectively.

The dependence of concentrations on the etch rates was not as significant as that of $HCl-HNO_3$ solution, as can be seen in Figure 14. The etch rates were about 100 times higher than that of dilute hydrochloric acid. Typical etch rates were 20 to 30 Å/s.

A problem of using dilute nitric acid for etching thin films was the inconsistency of the etching behavior: sometimes it etched sample films immediately after immersion, sometimes it had a time delay for a while and then suddenly etched the film, particularly for the case of much dilute solution. It should be noted that both concentrated nitric acid and hydrochloric acid showed passivity to Ni-Fe films at room temperatures.

a)

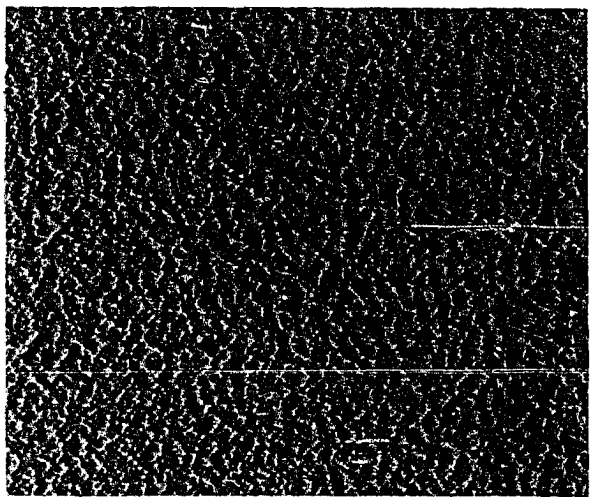

b)

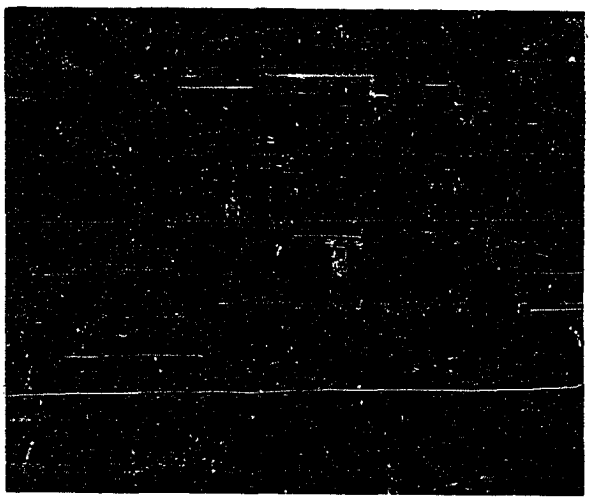

Figure 26. Electron micrographs of replicated film surfaces of
a) as-deposited film (83-17 Ni-Fe, 2000 Å, x 70,000)
b) etched film, 6000 sec. in dilute hydrochloric acid (x 70,000)

a)

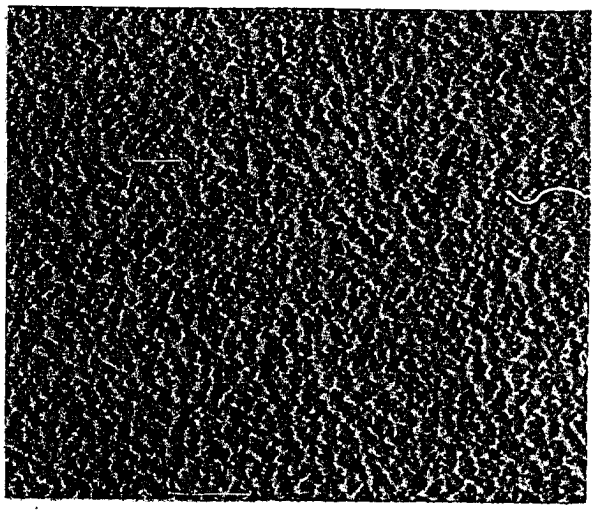

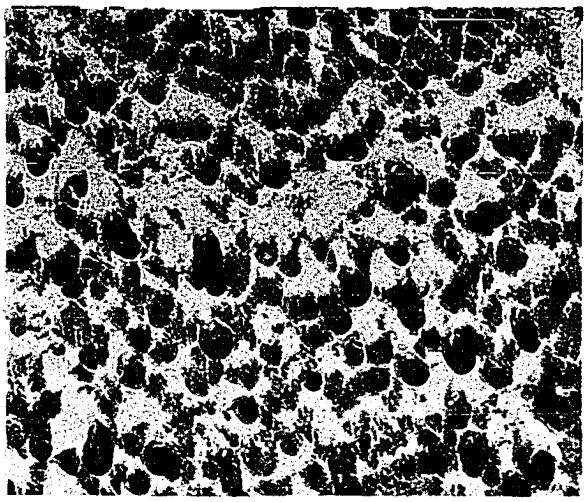

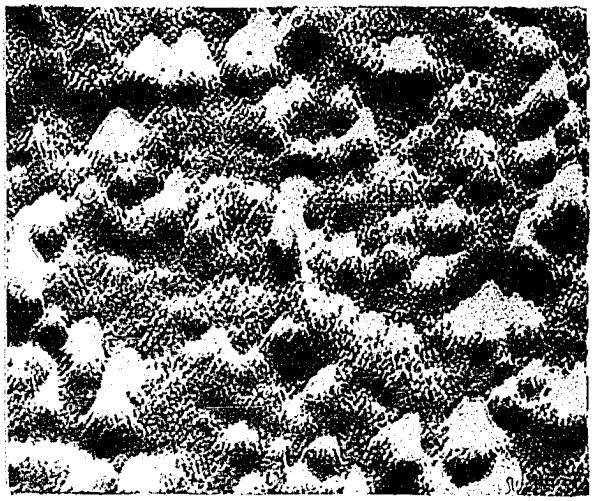

b)

c)

Figure 27. Electron micrographs of replicated film surfaces of
a) as-deposited film (83-17 Ni-Fe, 2000 Å, x 70,000)
b) etched film in 4% nitric acid for 41 sec. x 70,000
c) etched film in 10% nitric acid for 22 sec. x 70,000.

Effects of Ferric Chloride Acid

Ferric chloride solution has been known as the common reagent in photo-engraving and for heavy copper-clad circuit boards.

Ferric chloride solution (50 ml H_2O and 13.8 gr. of $FeCl_3 \cdot 6H_2O$) dissolved a 2000 Å Ni-Fe film in a few seconds. Being diluted in order to reduce the etch rates, the etching solution ran into a trouble of non-uniform wetting of the film surface. In addition to this, it exhibited the inconsistency of etching behavior experienced in nitric acid solution.

Effects of "Chemical Polish Solution for Ni and Ni Alloy"(51)

The Chemical Polish solution, which is claimed to give very good polish for nickel and nickel alloy at temperature of 85-95°C for 2-3 minutes, was tried on the sample films. When Ni-Fe films were etched at room temperatures, the solution produced a considerable amount of surface roughness as can be seen in Figure 28 b. For Ni-Fe-Co films, a very very rough surface was obtained by etching in Chemical Polish solution. Pictures taken by scanning electron microscope, as shown in Figure 28, reveals that the rough surface was actually an aggregate of dome-shaped particles produced by the etching. The changes in magnetic properties were: H_c = 1.5 Oe to 20 Oe, V_m = 220 mV to 120 mV, α_{90} = 0.5° to 22°, and H_k = 18 Oe to not measurable, where V_m is the height of the hysteresis loop. The thickness of as-deposited film was about 3000 Å. It must be noted that the particle size of the etched film was as large as 3000 Å in diameter or less. As a result, it provokes that the increase in H_c

and α_{90} were attributed to the formation of small particles throughout the film by preferential attack of the etching solution.

Effects of HNO_3+$FeCl_3$

As can be expected by considering the effects of both HNO_3 and $FeCl_3$ on the magnetic properties of films, the etching solution exhibited a very much similar etching behavior to the Chemical Polish solution. It produced a lot of very rough surfaces in a less etch time. Figure 29 b is an electron micrograph of replicated surface of Ni-Fe-Co films etched in this etchant and Figure 29 a is a picture taken by scanning electron microscope for the same film mentioned above. Both pictures manifest the film topography as an aggregate of small particles. One thing particular to this etchant was the limiting action as noted in Figure 19. The coercive force and angular dispersion were increased sharply and then leveled off. In this process the total magnetization flux was reduced less than 20%.

Since a unusually large increase in angular dispersion associated with HNO_3, $FeCl_3$, Chemical Polish, and HNO_3+$FeCl_3$ solution is not desirable from the device point of view, further investigations on those etching solutions were not pursued.

Effects of HCl+HNO_3+Copper

A small quantity of copper was dissolved in nitric acid followed by adding hydrochloric acid and water. The result was found to be encouraging in terms of surface roughness control. It produced, in many respects, very similar surface topography to that of nitric acid etching. However, the

a)

b)

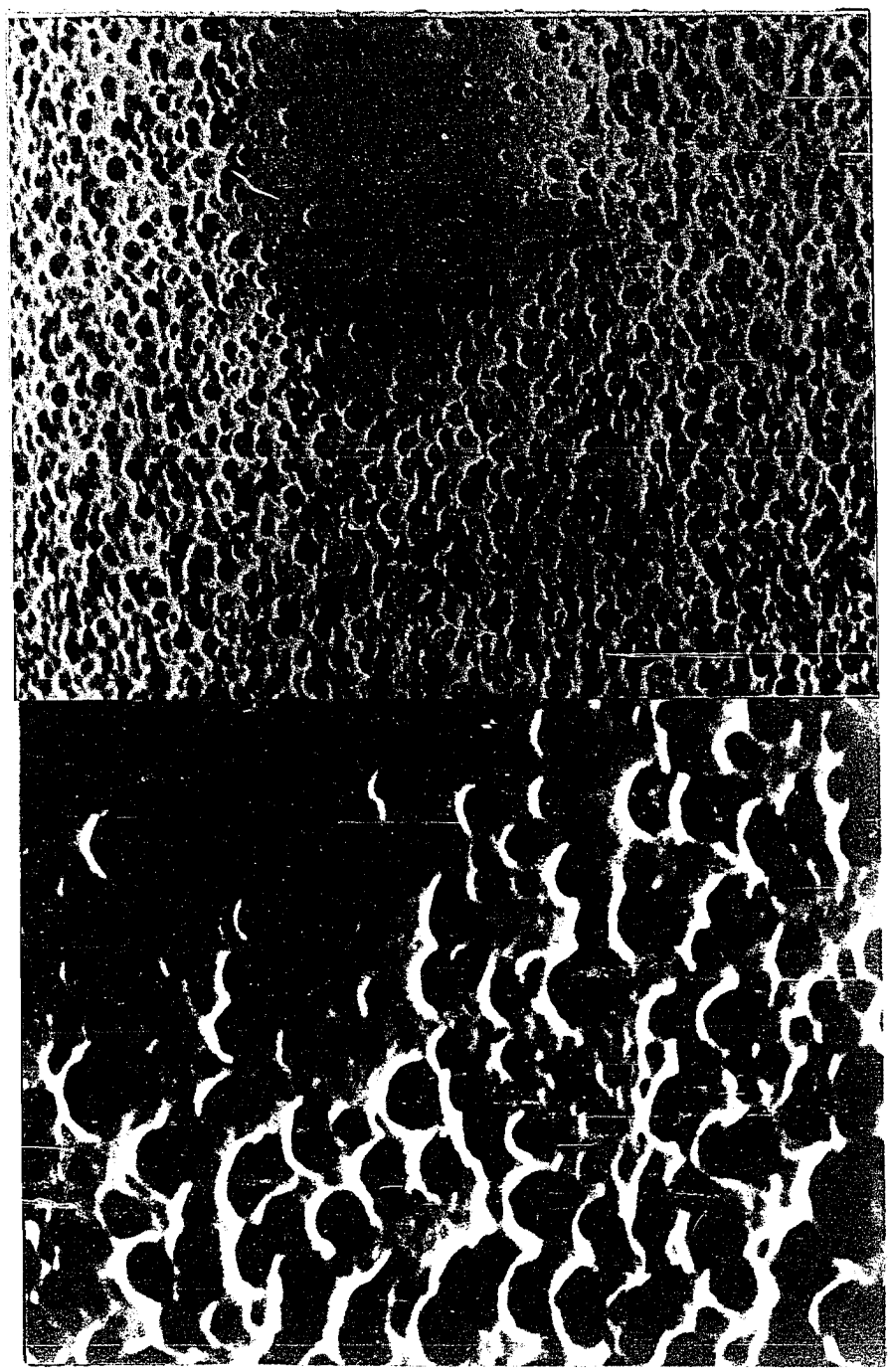

Figure 28. Scanning electron micrographs of 65-15-20 Ni-Fe-Co film (3000 Å)
a) etched for 135 sec. in the Chemical Polish, x 10,000
b) x 30,000

a)

b)

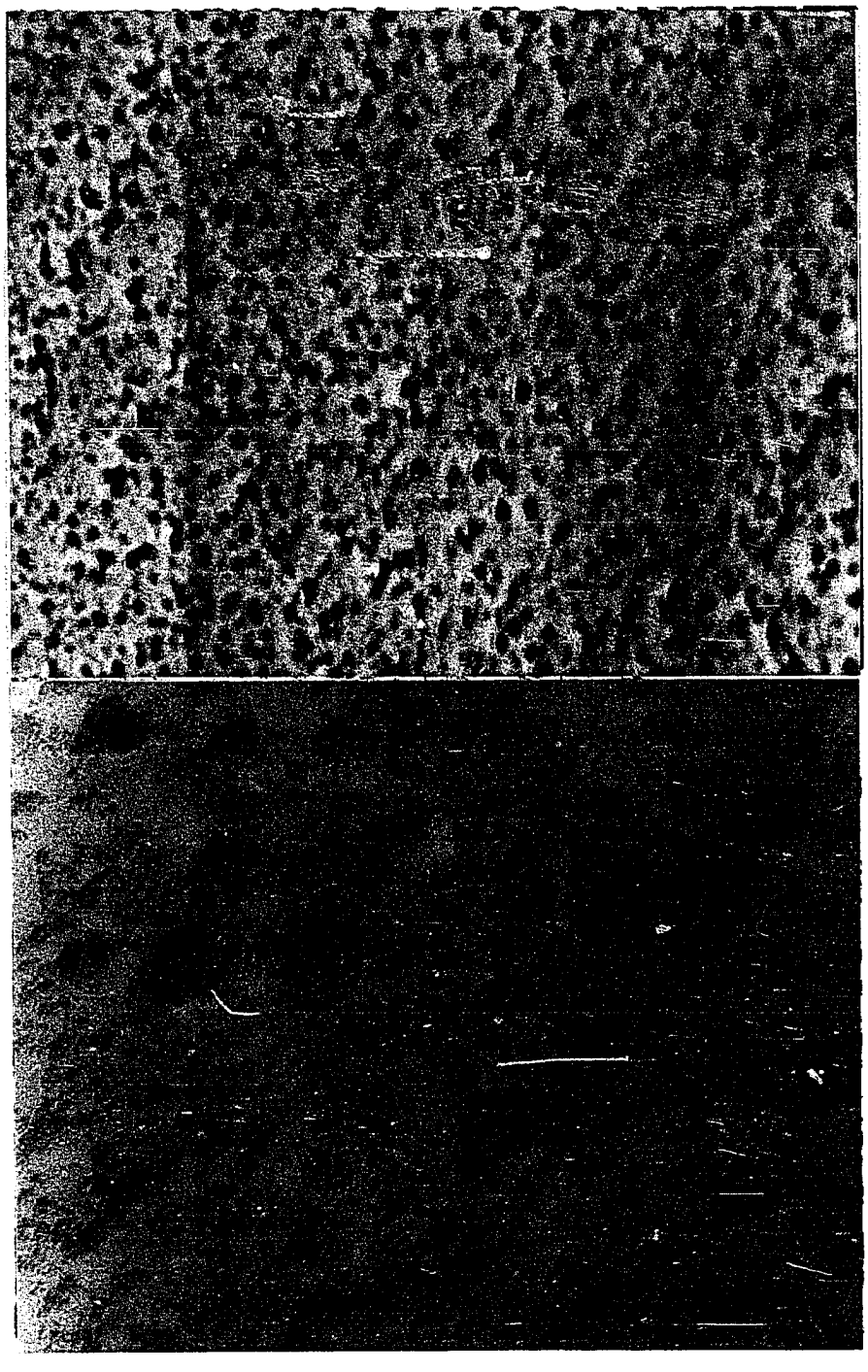

Figure 29. Ni-Fe-Co, 2000 Å in HNO_3+$FeCl_3$ solution for 14 seconds.
a) scanning electron micrograph (x 10,000)
b) electron micrograph (x 70,000), of an etched film (65-15-20)

a)

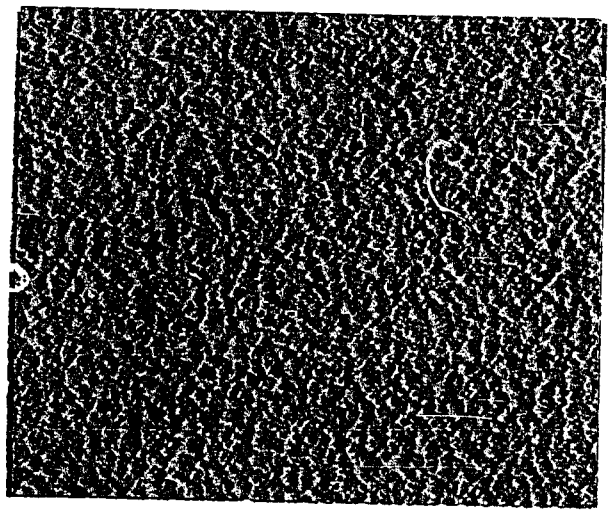

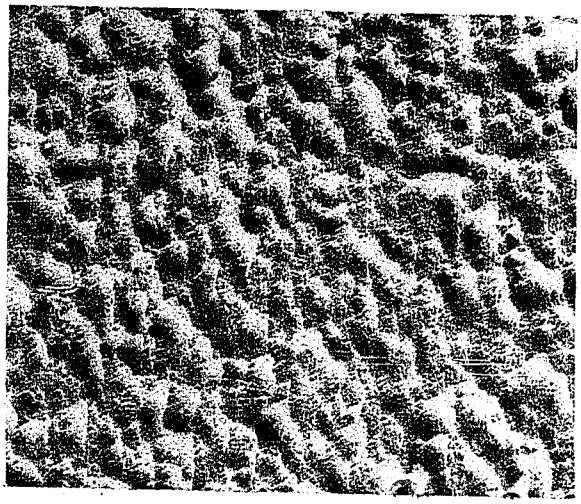

b)

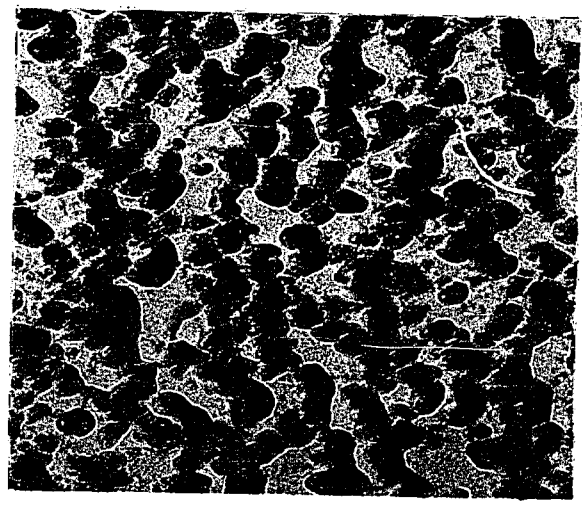

c)

Figure 30. Electron micrographs of replicated film surfaces of
a) as-deposited film (83-17 NiFe, 2000 A, x 70,000)
b) etched film (100 sec. in $HCl+HNO_3+Cu^{++}$, x 70,000)
c) etched film (370 sec. in $HCl+HNO_3+Cu^{++}$, x 70,000)

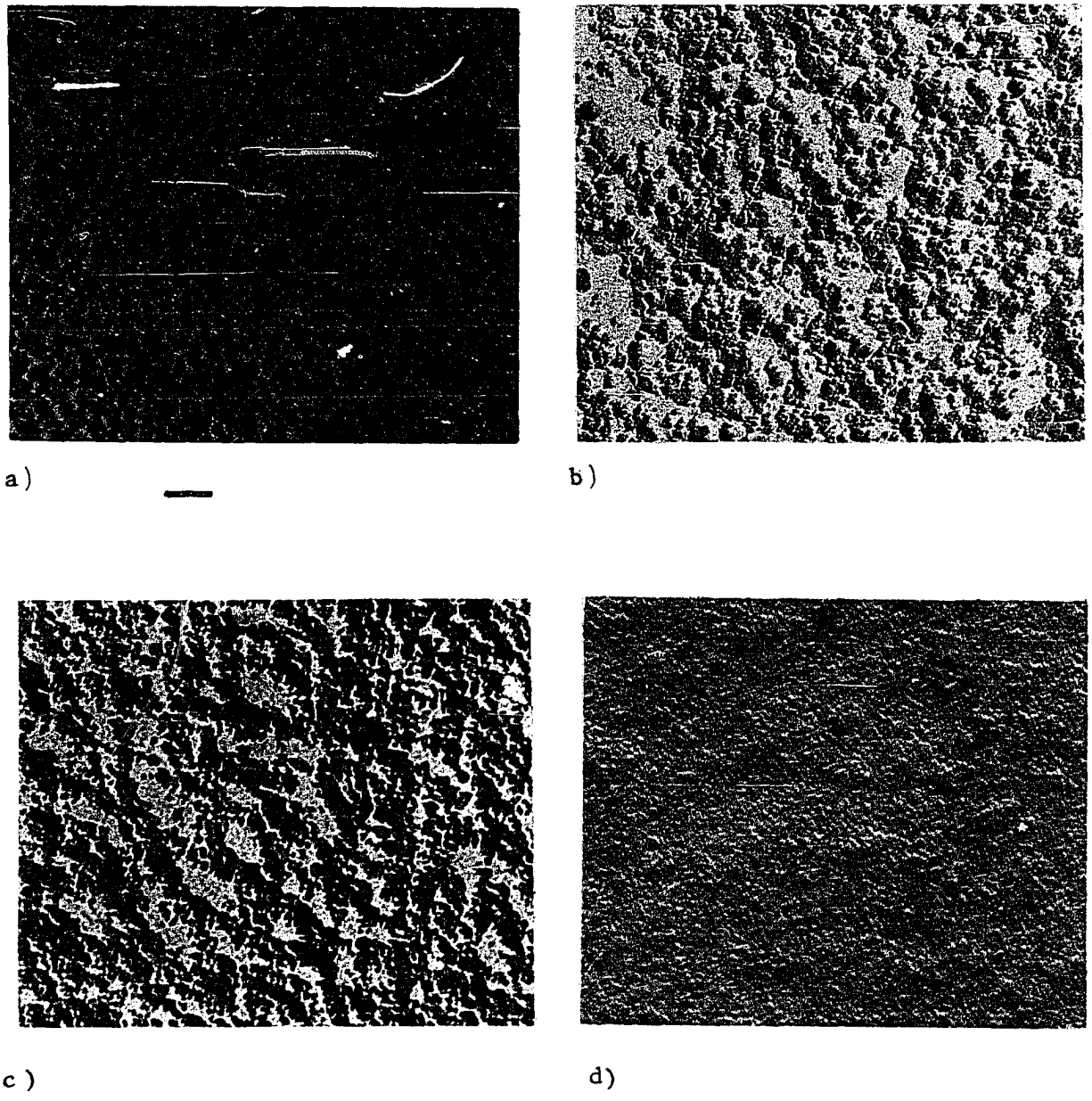

Figure 31. Electron micrographs of replicated film surfaces of
a) as-deposited film (83-17 Ni-Fe, 3000 Å, x 70,000)
b) etched film (777 sec. in the Chemical Polish, x 70,000)
c) etched film (1532 sec. in 20% $HCl+HNO_3$, x 70,000)
d) polished film of c) (alumina powder, 0.05μ dia.)

inconsistency observed in nitric acid solution did not appear in this composition. Also the etch rates were increased significantly from 0.3 Å/s to 5 Å/s. As shown in Figure 30, and the texture of surface roughness was different from that of $HCl+HNO_3$ solution. The variation of coercive force as a function of etch time is shown in Figure 19.

Polishing of Etched Surfaces of Films

Electron micographs of replicated surfaces of chemically etched films gave strong evidences that the thickness reduction and the surface roughness were mainly responsible for the increase in the coercive force and the angular dispersion by chemical etching. However, the possible artifacts which maybe present in electron microscopic investigations and other possible unknown surface phenomenon should not be overlooked. Thus, polishing of etched surface of films was employed as a method to check the possible etching mechanisms of chemical etching on magnetic thin films.

The surface of etched films was polished with the slurry of very fine alumina powder (0.05 μ diameter) which gives an effective scratch-free polishing. The effect of polishing on the magnetic properties of etched films is indicated by an arrow in Figures 17, 18, 19, and 20.

For example, an etched film (H_k = 3.5 Oe, H_c was increased from 1.2 Oe to 6 Oe, α_{90} increased from 2° to 15°, effective thickness from 2000 Å to 1000 Å, 83-17 Ni-Fe, in 20% $HCl+HNO_3$) was polished and the resulting changes in the magnetic properties were: the coercive force was decreased from 6 Oe to 3 Oe, and the angular dispersion from 15° to 4°. The effective film thickness was reduced only 100 Å from 1000 Å to 900 Å. It manifests

that the surface-induced magnetic inhomogeneities produced by chemical etching was virtually removed by polishing, since the effective thickness reduction by polishing was less than a 10% of the total thickness.

On the other hand, a film which was etched in HNO_3+$FeCl_3$ solution for 25 seconds (H_k = 3.5 Oe, H_c from 1.2 to 9 Oe, α_{90} from 2^o to 30^o?, 83-17 Ni-Fe, 2000 Å), was polished and the resulting changes in the magnetic properties were as follows; the coercive force was rather increased from 9 to 10 Oe, also α_{90} did similar increase. The total magnetization flux (the effective thickness) was reduced 20%. The most likely explanation of the result is that polishing could not smooth out the rough surface, since the structure of the etched film was appeared to be an aggregate of small magnetic particles, as depicted in the electron micrographs in Figure 29. As a consequence, it should be noted that HNO_3+$FeCl_3$ solution has a different etching mechanism, possibly strong diffuse-etch along grain boundaries of the film.

Even for the results of polishing etched films in 20% HCl+HNO_3 solution which gives more or less uniform removal of film thickness, the corresponding final values of the coercive force and the angular dispersion were a little bit larger than that of the same thickness of as-deposited films. It may be attributed to the fact that polishing cannot remove other inhomogeneities such as pinholes, and grain boundary diffuse-etch inside the volume of the film, etc.

DISCUSSION

A normalized coercive force h_c has been used as a very useful index of magnetization ripple or dispersion. Also, a plot of normalized coercive force vs. angular dispersion can be used as a useful measure for the quality of magnetic films for computer memory elements.

Figure 32 illustrates the variation of angular dispersion and normalized coercive force as a function of substrates temperature and film thickness, which is obtained from the data of 3% Co-Ni-Fe films. It is clearly shown that an increase of substrate temperatures has been one of the methods for fabricating films with $h_c \cong 1$ and with moderate angular dispersion. It is also easily seen that the film thickness has a predominant influence at higher substrate temperatures. It should be noted that the thickness dependence of coercive force is still observed in films with higher angular dispersion which is attributed to higher substrate temperatures. Therefore, optimum choice of substrate temperatures, surface roughness of substrate, and film thickness has been important for having a good quality of magnetic thin films for memory elements.

Another curve of h_c vs. α_{90} obtained from various papers is shown in Figure 33. Littwin's results achieved by Sn diffusion appears to be favorable to other results, in its storage properties of memory elements. However, diffusion of copper or tin was done on a relatively thin film thickness (500 Å for Cu, 600 Å for Sn). By considering the thickness dependence of coercive force, coercive force of films with metallic underlayers could be doubled. Consequently, films with metallic underlayers of 1000 Å thick, are compatible to films of nonmagnetic metal diffusions.

The results obtained by chemical etching were plotted in Figure 33. Its storage properties is found to be very close to Sn diffusion, or maybe better if the measuring technique of angular dispersion is taken into account; the induction loop method results in higher values of measured angular dispersion than that of Kerr-optic method.

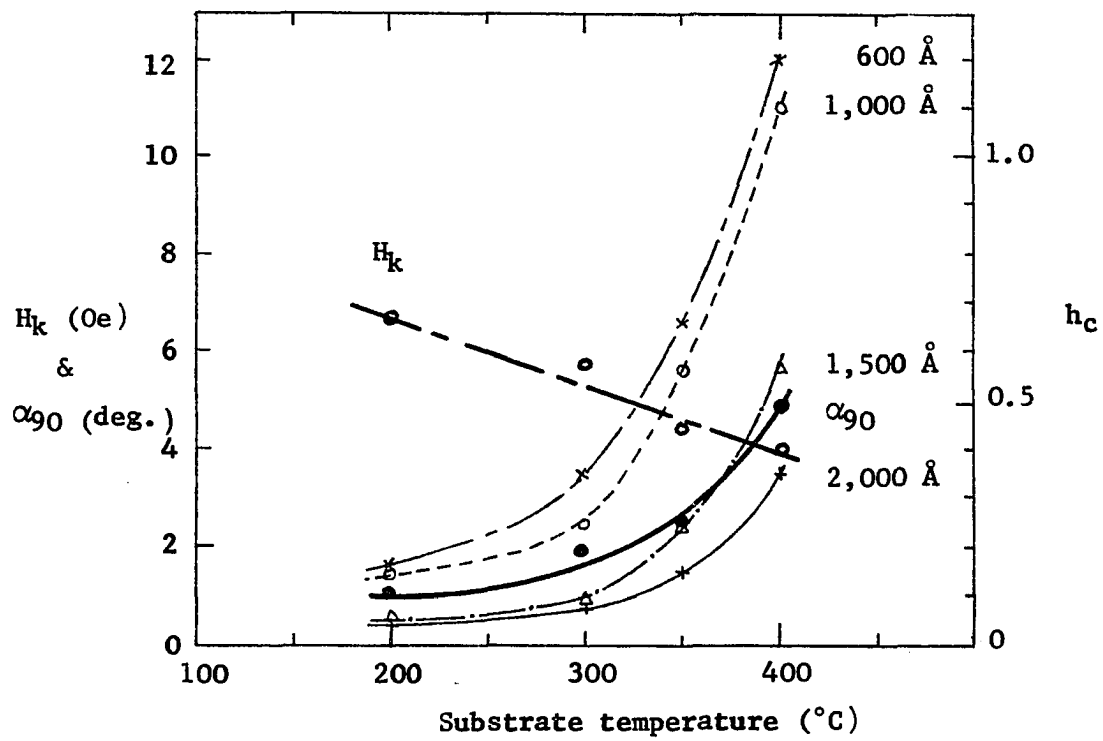

Figure 32. Variation of H_k, α_{90}, and h_c with substrate temperature and film thickness

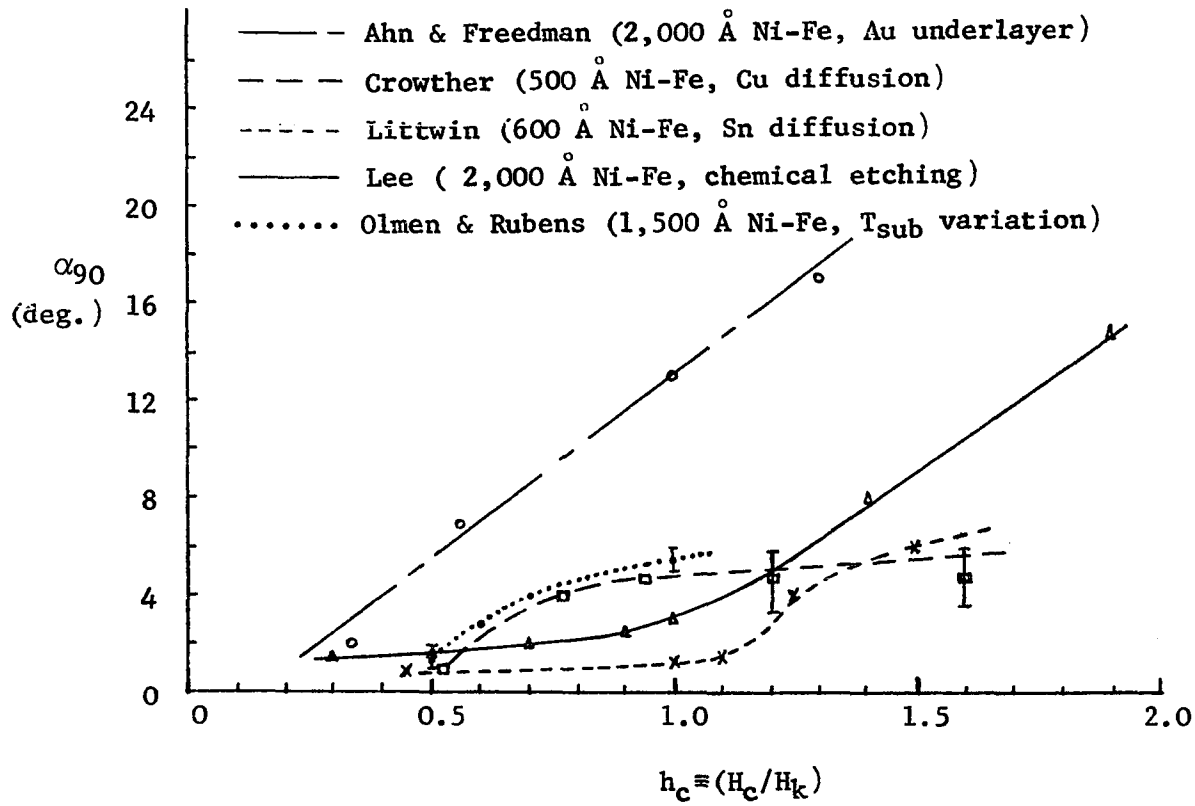

Figure 33. Comparison of the angular dispersion α_{90} for the films produced by different methods vs. the normalized coercive force

CONCLUSIONS

In this thesis the effects of chemical etching on the magnetic properties have been presented. Several different kind of etching solutions had been tried to investigate the effects of chemical etching in broad aspect. Examining the results of electron micrographs and polishing of etched film surfaces, it is clear that the thickness reduction and the microscopic surface roughness produced by chemical etching were mainly responsible for the increase in the coercive and the angular dispersion observed during the etch. Although the prominent factors influencing the magnetic properties appears to be the thickness reduction and the surface roughness as mentioned above, some other effects such as preferential etching of strain centers, voids, chemical inhomogeneities, grain boundary oxidation, and inclusions etc. should not be ignored.

During a normal chemical etching, grain boundary regions were revealed rather sharply as valley, since these regions possess higher free energy than the grain section proper. Thus, the initially smooth surface was modified to the rough surface having hills and valley structure.

An etched film has small-scale randomly shaped geometric inhomogeneities scattered throughout the surface of the film. The magnetic film will have corresponding regions of local ferromagnetic shape anisotropy, with randomly directed easy axis. The magnetization dispersion will accordingly be greater than that of as-deposited film. In other words, microscopic geometric inhomogeneities in a magnetic film can easily cause magnetic anisotropy effects due to the microscopic-shape anisotropy of the

inhomogeneities. As a result, the random local anistropy will be increased as the microscopic-shape anisotropy increases by chemical etching. When the random local anisotropy is increased by increasing the surface roughness by chemical etching, the angular dispersion and the coercive force increases. Also, the uniaxial character of the film becomes increasingly masked by the random local perturbing anisotropies and the magnetic behavior is increasingly determined by the latter.

It is observed that chemical etching may have several mechanisms. At first, it reduces film thickness, second, it produces microscopic surface roughness and finally, it may etch down through grain boundaries or voids. The contributions of these mechanisms may be dependent upon the choice of etching solution, its concentrations, etch time, temperature, and the structure of film itself.

It was, therefore, demonstrated that a proper selection of chemical etching solution could be used for improving the storage properties of magnetic thin films for computer memory elements. The results were compared with those of other techniques and found out to be compatible to Sn diffusion method which was claimed very good.

Side-products of this investigation are as follows; inverted films or modification of coercive force can be easily obtained by chemical etching; the contribution of the surface roughness to the coercive force and the angular dispersion can be easily demonstrated by polishing etched film surfaces with fine alumina powder; and Mirrofe solution cannot be used to check the thickness dependence of coercive force, particularly to prove 4/3 law; Mirrofe solution produces microscopic surface roughness, too.

LITERATURE CITED

1. Blois, M. S., Jr., "Preparation of Thin Magnetic Films and Their Properties,: J. Appl. Phys., 26, 975-980, 1955.

2. Ahn, K. Y., and Freedman, J. F., "Magnetic Properties of Vacuum-deposited Coupled Films," IBM J. Res. Develop., 12, 100-109, 1968.

3. Ahn, K. Y., and Freedman, J. F., "The Effects of Metallic Underlayers on Properties of Permalloy Films," IEEE Trans. Magnetics, MAG-3, 157-162, 1967.

4. Crowther, T. S., "The Effect of Cu Diffusion on the Magnetic Properties of Ni-Fe Films," Proc. INTERMAG, 2.8.1-2.8.5, 1965.

5. Littwin, B., "Improved Flat Ni-Fe Film Elements Obtained by Diffusion of an Electroplated Nonmagnetic Layer," IEEE Trans. Magnetics, MAG-5, 511-515, 1969.

6. Tiller, C. V., and Clark, G. W., "Coercive Force versus Thickness for Thin Films of Ni-Fe," Phys. Rev., 110, 583-585, 1958.

7. West, F. G., and Simmons, C. L., "Dependence of Angular Dispersion on Grain Size in Evaporated Permalloy Films," J. Appl. Phys., 37, 1283-1284, 1966.

8. Berkowitz, A. E., Shuele, W. J., and Morey, K. R., "Anisotropy Modifications and Domain-Wall Behavior in Grooved Films," IEEE Trans. Magnetics, MAG-6, 130-133, 1970.

9. Stoner, E. C., and Wohlfarth, E. P., "A Mechanism of Magnetic Hysteresis in Heterogeneous Alloys," Phil. Trans. Roy. Soc. London, 240A, 599-642, 1948.

10. Middelhoek, S., "Ferromagnetic Domains in Thin Ni-Fe Films," Drukkerij Wed. G. Van Soest N. V., Amsterdam, Holland, 1961.

11. Hoffman, H., "Theory of the Magnetization Ripple," IEEE Trans. Magnetics, MAG-4, 32-38, 1968.

12. Hart, K. J., "Theory of Magnetization Ripple in Ferromagnetic Films," J. Appl. Phys., 39, 1503-1524, 1968.

13. Maissel, L. I., and Glang, R. (eds.), Handbook of Thin Film Technology, New York, N. Y., McGraw-Hill, Inc., 1970.

14. Slonczewski, J. C., "Induced Anisotropy in Ni-Fe Films," IEEE Trans. Magnetics, MAG-4, 15-19, 1968.

15. Freedman, J. F., "Soft magnetic Thin-Film Memory Materials," IEEE Trans. Magnetics, MAG-5, 752-764, 1969.

16. Crowther, T. S., "Angular and Magnitude Dispersion of the Anisotropy in Magnetic Thin Films," J. Appl. Phys., 34, 580-587, 1963.

17. Tolman, C. H., and Oberg, P. E., "Dispersion of the Easy Axis in Permalloy Films as a Function of Deposition Parameters," Proc. INTERMAG, 12.3.1-12.3.4, 1963.

18. Cohen, M. S., "Influence of Anisotropy Dispersion on Magnetic Properties of Ni-Fe Films," J. Appl. Phys., 34, 1841-1847, 1963.

19. Rother, H., "Magnetische Eigenshaften Ferromagnetische Schichten. III," Z. Physik, 168, 283-291, 1962.

20. Brice, J. C., "The Effect of Inclusions on the Domain Coercive Force of Thin Ferromagnetic Films," British J. Appl. Phys., 16, 1523-1525, 1965.

21. Néel, L., "Remarques sûr la Théorie des Propriétés Magnétiques des Couches Minces et des Grains Fins," J. Phys. Radium, 17, 250-255, 1956.

22. Behrndt, K. H., and Maddocks, F. S., "Influence of Substrate Processing on the Magnetic Properties and Reproducibility of Evaporated Nickel-Iron Films," J. Appl. Phys., Suppl. 30, 276S-277S, 1959.

23. Bradley, E. M., "Properties of Magnetic Films for Memory Systems," J. Appl. Phys., Suppl. 33, 1051-1057, 1962.

24. Ahn, K. Y., and Freedman, J. F., "Magnetic Properties Observed During Vacuum Deposition of Permalloy Films," J. Appl. Phys., 37, 1481-1482, 1966.

25. Hanson, M. M., Norman, D. I., and Lo, D. S., "Stripe Domains in Ni-Fe Films with Zero and Positive Magnetostriction," Appl. Phys. Lett., 9, 99-100, 1966.

26. Pickard, R. M., Turner, J. A., Birtwistle, J. K., and Hoffman, C. R., "Thin Permalloy Films: Optimization of Properties of Computer Memories,: British J. Appl. Phys. (J. Phys. D.), 1, 1685-1696, 1968.

27. Bosnell, J. R., and Voisey, U. C., "An Assessment of Production Techniques for the Manufacture of Thin Ferromagnetic Films for Fast Computer Store Applications," Thin Solid Films, 4, 333-361, 1969.

28. Corres, J. M., and Hanson, M. M., "The Critical Thickness and Coercivity of Co-Ni-Fe Films," Appl. Phys. Lett., 12, 146-148, 1968.

29. Lemke, J. S., "Selected Glass Substrates and the Magnetic Parameters of the Films," Proc. INTERMAG., 12-2, 1963.

30. Prosen, R. J., Gran, B. E., and Kivel, J., "Effects of Surface Roughness of Magnetic Properties of Films," J. Appl. Phys., 34, 1147-1148, 1963.

31. Lesnik, A. G., Levin, G. I., and Kawarina, S. N., "The Influence of Roughness of the Substrates on the Coercive Force of Permalloy Films," Izv. Akad. Nauk. SSSR., 29, 594-598, 1965.

32. Mathias, J. S. and Fedde, G. A., "Plated-wire Technology: A Critical Review," IEEE Trans. Magnetics, MAG-5, 728-751, 1969.

33. Bozorth, R. M., Ferromagnetism, Princeton, New Jersey, D. Van Nostrand Co., 1956.

34. Uchiyama, S., Fujii, T., Masuda, M., and Sakaki, Y., "Origin of the Periodic Component of Anisotropy Dispersion in Ni-Fe Films II," Japan J. Appl. Phys., 6, 512-515, 1967.

35. Wiedermann, H., and Hoffmann, H., "Struktur and Krystallitgroesse Polykrystalliner Eisen- und Permalloy Schichten,: Z. Angew. Phys., 18, 502-506, 1965.

36. Fisher, R. D., and Haber, H. E., "Maximum Dispersion of the Easy Axis in Electrodeposited Thin Permalloy Films," Appl. Phys. Lett., 2, 11-12, 1963.

37. Iwata, T., Prosen, R. J., and Gran, B. E., "Magnetization Ripple in Multilayer Films," J. Appl. Phys., 38, 1364-1365, 1967.

38. Oredson, H. N., and Torok, E. J., "Causes of the Inhomogeneity in the Magnitude of Anisotropy Field in Thin Nickel-Iron Films," J. Appl. Phys., 36, 950-951, 1965.

39. Clow, H., "Variation of Anisotropy Axis Dispersion with Thickness of Nickel-Iron Films," Nature, 191, 996-997, 1961.

40. Leaver, K. D., "Dependence of the Anisotropy Axis Dispersion on Thickness of Thin Nickel-Iron-Cobalt Films," Nature, 196, 158-159, 1962.

41. Daughton, J. M., and Pohm, A. V., "Dispersion in Thin Magnetic Films," Proc. INTERMAG, 15.5.1-15.5.6, 1963.

42. Leaver, K. D., "Magnetization Ripple in Ferromagnetic Thin Films," Thin Solid Films, 2, 149-172, 1968.

43. Kehl, G. L., Principles of Metallographic Laboratory Practice, New York, N. Y., McGraw-Hill, Inc., 1949.

44. Smithells, C., Metals Reference Book, 4th ed., Vol. 1, London, Butterworths, Inc., 1967.

45. Prosen, R. J., Holman, J. O., and Gran, B. E., "Rotatable Anisotropy in Thin Permalloy Films," J. Appl. Phys., Suppl. 32, 91S-92S, 1961.

46. Prosen, R. J., Holman, J. O., Gran, B. E., and Cebulla, T. J., "Influence of Minor Constituents in Ferromagnetic Films," Proc. of International Conference on Magnetism and Crystallography, 1, 580-584, 1961.

47. Tsukahara, S., "Electron Microscopic Studies on Origins of Magnetization Ripples in Ferromagnetic Thin Films," J. Phys. Soc. of Japan, 23, 189-204, 1967.

48. Crowther, T. S., "Techniques for Measuring the Angular Dispersion of the Easy Axis of Magnetic Films," MIT London Laboratory Group Report 51-2, February 1959.

49. Kay, D. H., (ed.), Techniques for Electron Microscope, 2nd ed., Philadelphia, F. A. Davis Co., 1966.

50. Prosen, R. J., Holman, J. O., Gran, B. E., and Cebulla, T. J., "Stratification in Thin Permalloy Films," J. Appl. Phys., Suppl. 33, 1150-1151, 1962.

51. Tegart, W. J. McG., Electrolytic and Chemical Polishing of Metals in Research and Industry, London, Pergamon Press, 1956.

ACKNOWLEDGEMENT

The author wishes to express his sincere appreciation to his major professor, Dr. A. V. Pohm, for his constant encouragement and many valuable suggestions throughout the course of this study.

Also, thanks to Dr. C. S. Comstock for his help in operating the vacuum deposition systems and to Miss P. Mahoney for the electron micrographs of surface replicas of sample films.

A word of thanks is expressed to the National Science Foundation for the financial support of the study.

Finally, the author wishes to extend his special thanks to his family for their patience and understanding.